Stability of anisotropic magnetorheological elastomers in finite deformations: A micromechanical approach

Stephan Rudykh [a,*], Katia Bertoldi [b,c]

[a] Department of Mechanical Engineering, Massachusetts Institute of Technology, Cambridge, MA, USA
[b] School of Engineering and Applied Sciences, Harvard University, Cambridge, MA, USA
[c] Kavli Institute for Nanobio Science and Technology, Harvard University, Cambridge, MA, USA

ARTICLE INFO

ABSTRACT

We study the stability of magnetorheological elastomers (MREs) undergoing finite deformations in the presence of a magnetic field and derive a general condition for the onset of macroscopic instabilities. In particular, we focus on anisotropic MREs with magnetoactive particles that are aligned along a particular direction, forming chain-like structures. We idealize the microstructure of such anisotropic magnetosensitive elastomers as a multilayered structure and derive an analytical model for the behavior of these materials. The analytical model, together with the derived condition for the onset of instabilities, is used to investigate the influence of magnetomechanical finite deformations on the stability of the anisotropic MREs. While the formulation is developed for generic hyperelastic magnetosensitive elastomers, the results are presented for a special class of soft materials incorporating a neo-Hookean hyperelastic response. The influence of material properties and loading conditions is investigated, providing a detailed picture of the possible failure modes.

1. Introduction

Magnetorheological elastomers (MREs) consist of magnetic particles, such as micron-size iron particles, dispersed in an elastomeric matrix and can undergo large deformations when excited by a magnetic field. It is well known that application of an external magnetic field to MREs results in significant changes in their macroscopic properties (*e.g.*, Jolly et al., 1996; Ginder et al., 2000, 2002; Gong et al., 2005; Varga et al., 2006), so that they have been exploited to design tunable vibration absorbers and damping components (*e.g.*, Ginder et al., 2001; Deng et al., 2006; Lerner and Cunefare, 2008; Hoang et al., 2011), noise barrier system (Farshad and Le Roux, 2004) and sensors (Tian et al., 2011; Zadov et al., 2012).

Recent experiments (*e.g.*, Farshad and Benine, 2004; Danas et al., 2012) revealed that the microstructure of MREs has a strong impact on their macroscopic response. The distribution of the magnetic particles in MREs can be either random (and, consequently, nearly isotropic) or partially aligned by curing in the presence of a magnetic field (see Fig. 1(a) and (b)). The field-induced stiffening has been observed to be significantly increased in anisotropic MREs where the magnetoactive rigid particles are aligned and form chain-like structures (see Fig. 1). In particular, Chen et al. (2007) experimentally observed an increase of the incremental shear modulus for the samples prepared in the presence of higher magnetic fields, and consequently, with more pronounced chain-like microstructures.

---

* Corresponding author. Tel.: +1 617 253 5087
  E-mail address: rudykh@mit.edu (S. Rudykh).

ARTICLE IN PRESS

2   S. Rudykh, K. Bertoldi / J. Mech. Phys. Solids ▮ (▮▮▮▮) ▮▮▮–▮▮▮
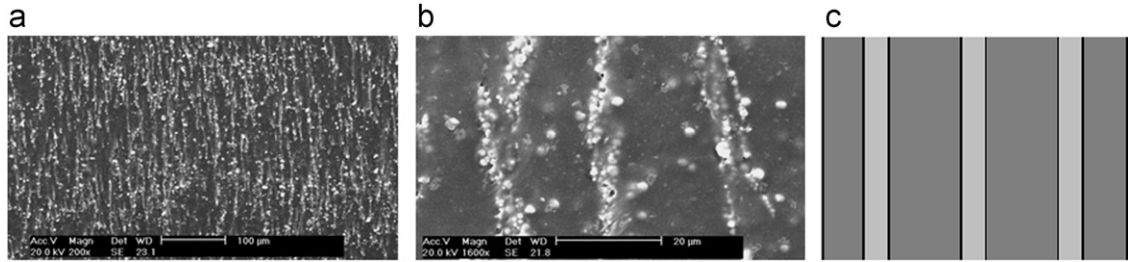
Fig. 1. (a) SEM image with 200 times magnification of MRE prepared in 800 mT (Chen et al., 2007); (b) SEM image with 1600 times magnification of MRE prepared in 800 mT (Chen et al., 2007); (c) schematic representation of the idealized layered microstructure considered in this work. (a) MRE (800 mT) X200. (b) MRE (800 mT) X1600. (c) Idealized MRE.

Theoretical and numerical models have been developed to unravel the mechanics of MREs. Motivated by the development of applications, the pioneering theory of electro and magneto-elastic macroscopic behavior of continuum proposed by Truesdell and Toupin (1960), Tiersten (1964, 1965), and Maugin and Eringen (1972) has been recently reviewed and further developed (Brigadnov and Dorfmann, 2003; Dorfmann and Ogden, 2004, 2005; Bustamante et al., 2006; Bustamante, 2010; Destrade and Ogden, 2011; Han et al., 2012; Thylander et al., 2012). In addition, a homogenization approach has been developed to identify the effective properties of MREs with random distribution of magnetoactive particles (Ponte Castañeda and Galipeau, 2011; Galipeau and Ponte Castañeda, 2012; Galipeau et al., forthcoming).

Since a limiting factor in the design of structures and composite materials is their failure under the applied loads, following the pioneering work of Hill (1957), the investigation of the stability of composites and structures subjected to purely mechanical loadings has attracted considerable attention (Biot, 1965; Hill and Hutchinson, 1975; Triantafyllidis and Maker, 1985; Fleck, 1997; Michel et al., 2007; Bertoldi and Boyce, 2008; Bruno et al., 2010; Rudykh and deBotton, 2012). Moreover, guided by well-established criteria for the "pure" mechanical case, the onset of instabilities for MRE with isotropic distributions of magnetic particles has been investigated focusing on surface instabilities of homogeneous magnetoactive half-space (Otténio et al., 2008) and failure modes of a rectangular MRE block undergoing plane–strain deformation in the presence of a magnetostatic field (Kankanala and Triantafyllidis, 2008).

Here, motivated by recent experiments (e.g., Chen et al., 2007; Guan et al., 2008; Danas et al., 2012), we focus on the stability of MREs with chain-like distributions of magnetic particles and introduce a micromechanical model to describe the behavior of the anisotropic media. To this end, we idealize the material as a multilayered structure (see Fig. 1(c)) and derive an analytical solution for the phase fields. Thus, the dependence of the overall behavior of the material on the volume fractions and material properties of the phases as well as the anisotropy direction is investigated. Next, we derive a general criterion for the onset of the coupled magnetoelastic macroscopic instabilities and further specialize it for the 2D case. By making use of this criterion, the macroscopic stability of multilayered hyperelastic MREs deforming at large strains is systematically investigated and closed form expressions for the identification of unstable domains along different loading paths are determined. We analyze the behavior of the anisotropic MREs in the presence of a magnetic field for three modes of finite deformations: (i) *simple shear in* 2D, (ii) *pure shear in* 2D and (iii) *axisymmetric shear in* 3D. Although the approach is not restricted to a specific choice of constitutive laws of the phases, here we present results for materials with neo-Hookean magnetoactive behavior of the constituents.

2. Theoretical background on magnetorheological elastomers

Let us consider a heterogeneous body and identify with $\mathcal{B}^0$ its undeformed configuration. The application of both mechanical loadings and magnetic fields deforms the body quasistatically from $\mathcal{B}^0$ to the current configuration $\mathcal{B}$. Such deformation is described by the function $\boldsymbol{\chi}$ that maps a reference point $\mathbf{x}^0$ in $\mathcal{B}^0$ to its deformed position $\mathbf{x} = \boldsymbol{\chi}(\mathbf{x}^0)$ in $\mathcal{B}$. The associated deformation gradient will be denoted by $\mathbf{F} = \partial \boldsymbol{\chi}/\partial \mathbf{x}^0$, while J identifies its determinant, $J = \det \mathbf{F}$.

In the absence of mechanical body forces and electric fields, and for deformations applied quasistatically, equilibrium of MREs is ensured when

$$\text{div } \boldsymbol{\sigma} = 0, \quad \text{div } \mathbf{B} = 0 \quad \text{and} \quad \text{curl } \mathbf{H} = 0, \tag{1}$$

where $\boldsymbol{\sigma}$ is the Cauchy total stress tensor, $\mathbf{B}$ is the Eulerian magnetic induction and $\mathbf{H}$ is the Eulerian magnetic field. Moreover, div(•) and curl(•) denote differential operators with respect to $\mathbf{x}$.

Eqs. (1) can be rewritten in terms of the total first Piola–Kirchhoff stress tensor $\mathbf{P} = J\boldsymbol{\sigma}\mathbf{F}^{-T}$, the Lagrangian magnetic field $\mathbf{H}^0 = \mathbf{F}^T\mathbf{H}$ and the Lagrangian magnetic induction $\mathbf{B}^0 = J\mathbf{F}^{-1}\mathbf{B}$ as

$$\text{Div } \mathbf{P} = 0, \quad \text{Div } \mathbf{B}^0 = 0 \quad \text{and} \quad \text{Curl } \mathbf{H}^0 = 0, \tag{2}$$

where Div(•) and Curl(•) are the differential operators with respect to $\mathbf{x}^0$.

ARTICLE IN PRESS

S. Rudykh, K. Bertoldi / J. Mech. Phys. Solids ▮ (▮▮▮▮) ▮▮▮–▮▮▮   3

Moreover, for a heterogenous infinite body the boundary conditions across interfaces separating different phases are given by

$$[\![\boldsymbol{\sigma}]\!] \cdot \mathbf{N} = 0, \quad \mathbf{N} \cdot [\![\mathbf{B}]\!] = 0 \quad \text{and} \quad \mathbf{N} \times [\![\mathbf{H}]\!] = 0 \tag{3}$$

or

$$[\![\mathbf{P}]\!] \cdot \mathbf{N}^0 = 0, \quad \mathbf{N}^0 \cdot [\![\mathbf{B^0}]\!] = 0 \quad \text{and} \quad \mathbf{N}^0 \times [\![\mathbf{H^0}]\!] = 0, \tag{4}$$

where $\mathbf{N} = \mathbf{F}^{-T}\mathbf{N}^0$ and $\mathbf{N}^0$ are the normals to the interface in the current and reference configurations, and the jump operator $[\![\bullet]\!] \equiv (\bullet)^+ - (\bullet)^-$ is defined such that $\mathbf{N}$ and $\mathbf{N}^0$ are pointing towards phase $(\bullet)^-$.

Finally, note that for a conservative material whose response is described by a free-energy–density function $\Psi(\mathbf{F},\mathbf{B^0})$

$$\mathbf{P} = \frac{\partial \Psi(\mathbf{F},\mathbf{B^0})}{\partial \mathbf{F}} \quad \text{and} \quad \mathbf{H^0} = \frac{\partial \Psi(\mathbf{F},\mathbf{B^0})}{\partial \mathbf{B^0}}. \tag{5}$$

For an incompressible material $(5)_1$ modifies as

$$\mathbf{P} = \frac{\partial \Psi(\mathbf{F},\mathbf{B^0})}{\partial \mathbf{F}} - p\mathbf{F}^{-T}, \tag{6}$$

where p is a pressure-like Lagrange multiplier.

3. Incremental equations

Following the approach recently developed to investigate instabilities in electroactive composites (Dorfmann and Ogden, 2010; Bertoldi and Gei, 2011; Rudykh and deBotton, 2011), we derive the governing equations for the incremental deformations superimposed upon a given state of finite deformation in the presence of a magnetic field. The incremental problem is defined by

$$\text{Div } \dot{\mathbf{P}} = 0, \quad \text{Div } \dot{\mathbf{B}}^0 = 0 \quad \text{and} \quad \text{Curl } \dot{\mathbf{H}}^0 = 0, \tag{7}$$

where $\dot{\mathbf{P}}$, $\dot{\mathbf{B}}^0$ and $\dot{\mathbf{H}}^0$ are infinitesimal changes in the nominal stress, magnetic induction and magnetic field, respectively.

Assuming that all incremental quantities are sufficiently small, the constitutive relations (5) can be linearized as

$$\dot{P}_{ij} = \mathcal{A}^0_{ijkl}\dot{F}_{kl} + \mathcal{M}^0_{ijk}\dot{B}^0_k \quad \text{and} \quad \dot{H}^0_i = \mathcal{M}^0_{jki}\dot{F}_{jk} + \mathcal{H}^0_{ij}\dot{B}^0_j, \tag{8}$$

where the magnetoelastic moduli tensors are given by

$$\mathcal{A}^0_{i\alpha k\beta} = \frac{\partial^2 \Psi}{\partial F_{i\alpha}\partial F_{k\beta}}, \quad \mathcal{M}^0_{i\alpha\beta} = \frac{\partial^2 \Psi}{\partial F_{i\alpha}\partial B^0_\beta} \quad \text{and} \quad \mathcal{H}^0_{\alpha\beta} = \frac{\partial^2 \Psi}{\partial B^0_\alpha \partial B^0_\beta}. \tag{9}$$

Note that for an incompressible material the linearized constitutive relation for the incremental stress tensor modifies as

$$\dot{P}_{ij} = \mathcal{A}^0_{ijkl}\dot{F}_{kl} + \mathcal{M}^0_{ijk}\dot{B}^0_k - \dot{p}F^{-1}_{ji} + pF^{-1}_{jk}\dot{F}_{kl}F^{-1}_{li}, \tag{10}$$

where $\dot{p}$ is the incremental change in p.

For further analysis of instabilities it is convenient to reformulate the incremental boundary value problem in an updated Lagrangian formulation, where the reference configuration moves and is identified with the current configuration. The push forward transformations of $\dot{\mathbf{P}}$, $\dot{\mathbf{H}}^0$ and $\dot{\mathbf{B}}^0$ to the current configuration are

$$\hat{\mathbf{T}} = J^{-1}\dot{\mathbf{P}}\mathbf{F}^T, \quad \hat{\mathbf{B}} = J^{-1}\mathbf{F}\dot{\mathbf{B}}^0, \quad \hat{\mathbf{H}} = \mathbf{F}^{-T}\dot{\mathbf{H}}^0, \tag{11}$$

with $\dot{\mathbf{F}} = (\text{grad } \mathbf{v})\mathbf{F}$, $v_i = \dot{x}_i$ denoting an incremental displacement.

Substitution of the incremental updated quantities into the governing equations (7) yields

$$\text{div } \hat{\mathbf{T}} = 0, \quad \text{div } \hat{\mathbf{B}} = 0 \quad \text{and} \quad \text{curl } \hat{\mathbf{H}} = 0. \tag{12}$$

Moreover, substitution of (11) into (8) yields

$$\hat{T}_{ij} = \mathcal{A}_{ijkl}v_{k,l} + \mathcal{M}_{ijk}\hat{B}_k - \dot{p}\delta_{ij} + pv_{j,i}, \quad \hat{H}_i = \mathcal{M}_{jki}v_{j,k} + \mathcal{H}_{ij}\hat{B}_j, \tag{13}$$

where

$$\mathcal{A}_{ijkl} = J^{-1}F_{j\alpha}F_{l\beta}\mathcal{A}^0_{i\alpha k\beta}, \quad \mathcal{M}_{ijk} = F_{j\alpha}F^{-1}_{\beta k}\mathcal{M}^0_{i\alpha\beta}, \quad \mathcal{H}_{ij} = JF^{-1}_{\alpha i}F^{-1}_{\beta j}\mathcal{H}^0_{\alpha\beta}. \tag{14}$$

Note that the updated magnetoelastic moduli possess symmetries

$$\mathcal{A}_{ijkl} = \mathcal{A}_{klij}, \quad \mathcal{M}_{ijk} = \mathcal{M}_{jik}, \quad \mathcal{H}_{ij} = \mathcal{H}_{ji}. \tag{15}$$

ARTICLE IN PRESS

4   *S. Rudykh, K. Bertoldi / J. Mech. Phys. Solids ▮ (▮▮▮▮) ▮▮▮–▮▮▮*

Finally, upon substitution of the linearized relations (13) into (12), the following equations are obtained:

$$\mathcal{A}_{ijkl}v_{k,lj} + \mathcal{M}_{ijk}\hat{B}_{k,j} - \dot{p}_{,i} = 0 \quad \text{and} \quad \epsilon_{spi}(\mathcal{M}_{jki}v_{j,kp} + \mathcal{H}_{ij}\hat{B}_{j,p}) = 0, \tag{16}$$

where ϵ_{spi} is the Levi–Civita permutation tensor.

4. Onset of macroscopic instabilities

Long-wavelength or macroscopic instabilities are known to be of particular prominence in fiber-reinforced elastomers (Triantafyllidis and Maker, 1985). In the mechanics of non-linear composites (Geymonat et al.,1993) showed that macroscopic instabilities occur when the homogenized properties lose strong ellipticity. Extending the formulation presented by Hill and Hutchinson (1975) for the pure mechanical case and following the recent works by Bertoldi and Gei (2011), Rudykh and deBotton (2011), and Destrade and Ogden (2011), we seek for a solution of (16) in the form of a standing plane wave, namely

$$v_i = \tilde{v}_i f(\mathbf{a} \cdot \mathbf{x}), \quad \dot{p} = \tilde{q}(\mathbf{a} \cdot \mathbf{x}), \quad \hat{B}_i = \tilde{b}_i g(\mathbf{a} \cdot \mathbf{x}), \tag{17}$$

where f and g are sufficiently continuously differentiable functions and $\mathbf{a}$ is a unit vector. Substitution of relations (17) into (16) yields

$$Q_{ik}\tilde{v}_k f'' + R_{ik}\tilde{b}_k g' - a_i \tilde{q}' = 0 \tag{18}$$

and

$$\epsilon_{spi}(R_{ji}\tilde{v}_j f'' + \mathcal{H}_{ij}\tilde{b}_j g')a_p = 0, \tag{19}$$

where $Q_{ik} = \mathcal{A}_{ijkl}a_j a_l$ is the acoustic tensor and $R_{ik} = \mathcal{M}_{ijk}a_j$. It follows from (19) that

$$\mathbf{s} - (\mathbf{s} \cdot \mathbf{a})\mathbf{a} = \mathbf{0}, \tag{20}$$

with $\mathbf{s} = \mathbf{R}^T\tilde{\mathbf{v}}f'' + \mathcal{H}\tilde{\mathbf{b}}g'$. By taking the dot product of (20) with $\tilde{\mathbf{b}}$ and noting that Eq. (12)$_2$ requires

$$\tilde{\mathbf{b}} \cdot \mathbf{a} = 0, \tag{21}$$

we obtain

$$g' = -\frac{\tilde{\mathbf{b}} \cdot \mathbf{R}^T\tilde{\mathbf{v}}}{\tilde{\mathbf{b}} \cdot \mathcal{H}\tilde{\mathbf{b}}}f''. \tag{22}$$

Finally, substituting (22) into (18) and taking the dot product with $\tilde{\mathbf{v}}$ we obtain

$$(\mathbf{Q}\tilde{\mathbf{v}}) \cdot \tilde{\mathbf{v}} - \frac{(\tilde{\mathbf{v}} \cdot \mathbf{R}\tilde{\mathbf{b}})(\tilde{\mathbf{b}} \cdot \mathbf{R}^T\tilde{\mathbf{v}})}{\tilde{\mathbf{b}} \cdot \mathcal{H}\tilde{\mathbf{b}}} = 0, \tag{23}$$

since the incompressibility constraint requires

$$\tilde{\mathbf{v}} \cdot \mathbf{a} = 0. \tag{24}$$

Hence, macroscopic instabilities may develop whenever the condition

$$(\mathbf{Q}\tilde{\mathbf{v}}) \cdot \tilde{\mathbf{v}} - \frac{(\tilde{\mathbf{v}} \cdot \mathbf{R}\tilde{\mathbf{b}})(\tilde{\mathbf{b}} \cdot \mathbf{R}^T\tilde{\mathbf{v}})}{\tilde{\mathbf{b}} \cdot \mathcal{H}\tilde{\mathbf{b}}} > 0 \tag{25}$$

is first violated along any arbitrary loading path, for any $\tilde{\mathbf{v}}$, $\tilde{\mathbf{b}}$, and $\mathbf{a}$ subjected to the conditions (21) and (24). Note that condition (25) is equivalent to the criterion derived by Destrade and Ogden (2011) for propagation of magneto-elastic infinitesimal homogeneous plane waves.

Furthermore, for a 2D problem the critical condition (23) can be explicitly written in terms of a sextic polynomial equation for $\xi \equiv a_2/a_1$, namely

$$\Gamma_6\xi^6 + \Gamma_5\xi^5 + \Gamma_4\xi^4 + \Gamma_3\xi^3 + \Gamma_2\xi^2 + \Gamma_1\xi + \Gamma_0 = 0, \tag{26}$$

where coefficients Γ_i are given by (A.4) in Appendix A. The details of the derivation of Eq. (26) are provided in Appendix A.

Thus, a macroscopic instability may occur when a real solution ξ of (26) exists. We note that the general condition (23) and its specialization to 2D conditions (26) can be used for the analysis of instability in *multiphase* hyperelastic magnetosensitive materials employing the pertinent homogenized constitutive moduli obtained either numerically or via a homogenization procedure.

5. MREs with layered microstructures

Recent experiments (*e.g.,* Farshad and Benine, 2004; Danas et al., 2012) revealed that the microstructure of MREs has a strong impact on their macroscopic response. In particular, the field-induced stiffening has been observed to be significantly increased in anisotropic MREs where the magnetoactive rigid particles are aligned and form chain-like structures (see Fig. 1). In order to account for the anisotropy and to investigate analytically through exact and explicit

ARTICLE IN PRESS

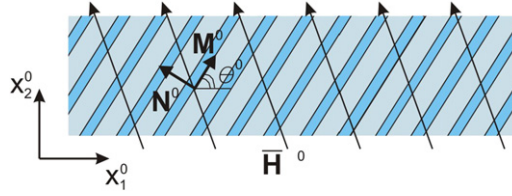*S. Rudykh, K. Bertoldi / J. Mech. Phys. Solids ▮ (▮▮▮▮) ▮▮▮–▮▮▮*   5

Fig. 2. Schematic representation of an anisotropic multilayered MRE.

formulae the influence on the overall material response of both spacial and material parameters as well as of coupled loading conditions, here we focus on MREs with layered microstructures. Note that for this specific case, the boundary value problems can be solved *exactly* even in the frame of finite deformations.

Let us consider a heterogeneous composite with layered microstructures (see Fig. 2). The constituents are *incompressible* magnetosensitive elastomers with volume fractions $c^{(m)}$ and $c^{(i)} = 1 - c^{(m)}$. Here and thereafter, the fields and parameters characterizing stiff and soft phases are denoted by superscripts $(\bullet)^{(i)}$ and $(\bullet)^{(m)}$, respectively. We denote by $\mathbf{N}^0$ the direction normal to the layers plane (*i.e.*, the laminate direction), while $\mathbf{M}^0$ is a unit vector tangent to the interface, both in the undeformed configuration. The vectors can be expressed in terms of the referential lamination angle Θ^0 as

$$\mathbf{N}^0 = \sin \Theta^0 \, \mathbf{e}_1 + \cos \Theta^0 \, \mathbf{e}_2 \quad \text{and} \quad \mathbf{M}^0 = \cos \Theta^0 \, \mathbf{e}_1 - \sin \Theta^0 \, \mathbf{e}_2. \tag{27}$$

5.1. Homogenization of multilayered MREs

Since the onset of macroscopic instabilities is detected by analyzing the homogenized properties of the composite, we start with homogenizing the multilayered MRE. For a multilayered material where all fields are homogeneous in each phase, the macroscopic deformation gradient $\overline{\mathbf{F}}$, the macroscopic Lagrangian magnetic field $\overline{\mathbf{H}}^0$ and the macroscopic magnetic induction $\overline{\mathbf{B}}^0$ are defined as

$$\overline{\mathbf{F}} = c^{(m)}\mathbf{F}^{(m)} + c^{(i)}\mathbf{F}^{(i)}, \quad \overline{\mathbf{H}}^0 = c^{(m)}\mathbf{H}^{0(m)} + c^{(i)}\mathbf{H}^{0(i)} \quad \text{and} \quad \overline{\mathbf{B}}^0 = c^{(m)}\mathbf{B}^{0(m)} + c^{(i)}\mathbf{B}^{0(i)}. \tag{28}$$

The deformation gradient in each phase can be obtained by making use of the displacement continuity condition across the interface (*i.e.*, $\mathbf{F}^{(m)}\mathbf{M}^0 = \mathbf{F}^{(i)}\mathbf{M}^0$) as (see deBotton, 2005 for details)

$$\mathbf{F}^{(m)} = \overline{\mathbf{F}}(\mathbf{I} + c^{(i)}\alpha\mathbf{M}^0 \otimes \mathbf{N}^0) \quad \text{and} \quad \mathbf{F}^{(i)} = \overline{\mathbf{F}}(\mathbf{I} - c^{(m)}\alpha\mathbf{M}^0 \otimes \mathbf{N}^0), \tag{29}$$

where the scalar α is obtained from the traction continuity condition equations $(4)_1$. Moreover, the continuity condition for the Lagrangian magnetic induction equations $(4)_2$ can be recast as

$$\mathbf{B}^{0(m)} - \mathbf{B}^{0(i)} = \beta\mathbf{M}^0. \tag{30}$$

Introduction of Eq. (30) into Eq. $(28)_3$ yields

$$\mathbf{B}^{0(m)} = \overline{\mathbf{B}}^0 + c^{(i)}\beta\mathbf{M}^0 \quad \text{and} \quad \mathbf{B}^{0(i)} = \overline{\mathbf{B}}^0 - c^{(m)}\beta\mathbf{M}^0, \tag{31}$$

where β is a scalar to be determined from the continuity condition for the Lagrangian magnetic field equation $(4)_3$, namely

$$(\mathbf{H}^{0(m)} - \mathbf{H}^{0(i)}) \cdot \mathbf{M}^0 = 0. \tag{32}$$

Eqs. (29), (31) and (32) together with constitutive relations of the phases (see Section 6.1) define a solution of the boundary value problem.

Furthermore, the total energy–density function of the composite can be expressed as the weighted sum of phase energy–density functions, namely

$$\overline{\Psi}(\overline{\mathbf{F}}, \overline{\mathbf{B}}^0) = \sum_{r = m,i} c^{(r)} \Psi^{(r)}(\overline{\mathbf{F}}, \overline{\mathbf{B}}^0) \tag{33}$$

and the macroscopic nominal stress tensor and Lagrangian magnetic field can be obtained as

$$\overline{\mathbf{P}} = \frac{\partial \overline{\Psi}}{\partial \overline{\mathbf{F}}} - p\overline{\mathbf{F}}^{-T} \quad \text{and} \quad \overline{\mathbf{H}}^0 = \frac{\partial \overline{\Psi}}{\partial \overline{\mathbf{B}}^0}. \tag{34}$$

Finally, explicit expressions for the macroscopic effective magnetoelastic moduli can be calculated as

$$\overline{\mathcal{A}}^0 = \frac{\partial^2 \overline{\Psi}}{\partial \overline{\mathbf{F}} \partial \overline{\mathbf{F}}}, \quad \overline{\mathcal{M}}^0 = \frac{\partial^2 \overline{\Psi}}{\partial \overline{\mathbf{F}} \partial \overline{\mathbf{B}}^0} \quad \text{and} \quad \overline{\mathcal{H}}^0 = \frac{\partial^2 \overline{\Psi}}{\partial \overline{\mathbf{B}}^0 \partial \overline{\mathbf{B}}^0}. \tag{35}$$

ARTICLE IN PRESS

6   S. Rudykh, K. Bertoldi / J. Mech. Phys. Solids ▮ (▮▮▮▮) ▮▮▮–▮▮▮

6. Results for multilayered MREs

Here, we investigate the non-linear response of anisotropic MREs with layered microstructure and identify the onset of macroscopic instabilities for three relevant loading conditions, namely simple and pure shear in 2D and axisymmetric shear in 3D in the presence of a magnetic field. Results will be presented for MREs whose response is captured by using an extended neo-Hookean form for the energy–density function. Although we are interested in the response of elastomers with magnetic filler particles mainly localized in chain-like structures, Fig. 1 clearly shows that the magnetoactive particles are also distributed in the soft layers between the chains. Consequently, also the soft phase is assumed to be magnetoactive (i.e., $\mu^{(m)} > 1$, $\mu^{(i)} > \mu^{(m)}$) and we focus on multilayered materials characterized by a contrast ratio of the phases material constants $G^{(i)}/G^{(m)} = \mu^{(i)}/\mu^{(m)} = 10$ and 100.

6.1. Constituent material properties

In the following sections results are presented for incompressible MREs phases whose response is captured using an extended neo-Hookean energy–density function. Moreover, we assume a linear constitutive relation between magnetic field and magnetic induction, namely

$$\mathbf{B} = \mu\mu_0\mathbf{H}, \tag{36}$$

where μ is a constant[1] and μ_0 is the magnetic permeability of vacuum.[2]

The response of isotropic magnetoactive materials can be captured by using a decoupled energy–density function (Ponte Castañeda and Galipeau, 2011), namely

$$\Psi(\mathbf{F},\mathbf{B^0}) = \Psi_{mech}(\mathbf{F}) + \frac{1}{2\mu_0\mu J}(\mathbf{FB^0})\cdot(\mathbf{FB^0}), \tag{38}$$

where $\Psi_{mech}(\mathbf{F})$ represents a purely mechanical contribution. In particular, for the incompressible MREs whose response is captured by using a neo-Hookean form for the mechanical free-energy–density function, Eq. (38) can be specialized as

$$\Psi(\mathbf{F},\mathbf{B^0}) = \frac{G}{2}(\mathrm{Tr}\,\mathbf{C}-3) + \frac{1}{2\mu_0\mu J}(\mathbf{FB^0})\cdot(\mathbf{FB^0}), \tag{39}$$

where $\mathbf{C} \equiv \mathbf{F}^T\mathbf{F}$ is the right Cauchy–Green strain tensor and G is the initial shear modulus. The corresponding total first Piola–Kirchhoff stress tensor and Lagrangian magnetic field are then obtained from Eqs. (5) as

$$\mathbf{P} = G\mathbf{F} + \frac{(\mathbf{FB^0})\otimes\mathbf{B^0}}{\mu_0\mu} - p\mathbf{F}^{-T} \tag{40}$$

and

$$\mathbf{H^0} = \frac{\mathbf{F}^T(\mathbf{FB^0})}{\mu\mu_0}, \tag{41}$$

respectively.

Moreover, for a multilayered structure whose phases are characterized by the energy–density function (39), the constants α and β entering in the homogenized response (Eqs. (29)–(32)) can be determined explicitly as

$$\alpha = \frac{G^{(i)}-G^{(m)}}{c^{(m)}G^{(i)}+c^{(i)}G^{(m)}}\frac{\overline{\mathbf{F}}\mathbf{N}^0\cdot\overline{\mathbf{F}}\mathbf{M}^0}{\overline{\mathbf{F}}\mathbf{M}^0\cdot\overline{\mathbf{F}}\mathbf{M}^0} \tag{42}$$

and

$$\beta = \frac{\mu^{(m)}G^{(m)}-\mu^{(i)}G^{(i)}}{(c^{(m)}G^{(i)}+c^{(i)}G^{(m)})\overline{\mu}}\frac{\overline{\mathbf{F}}\,\overline{\mathbf{B}}^0\cdot\overline{\mathbf{F}}\mathbf{M}^0}{\overline{\mathbf{F}}\mathbf{M}^0\cdot\overline{\mathbf{F}}\mathbf{M}^0} + \frac{G^{(i)}-G^{(m)}}{c^{(m)}G^{(i)}+c^{(i)}G^{(m)}}\overline{\mathbf{B}}^0\cdot\mathbf{M}^0, \tag{43}$$

where $\overline{\mu} = (c^{(m)}\mu^{(m)}+c^{(i)}\mu^{(i)})\mu_0$.

---

[1] Although, for the sake of simplicity, here we consider μ to be constant, the saturation effect occurring at high magnetic fields can be easily included by having μ to be a function of the magnetic field, $\mu(\overline{\mathbf{H}})$. Functions to capture the saturation effect can be easily constructed and an example is given by

$$\mu(H) = \mu^*\left(1 + \aleph(H_s)\left(\frac{H_s}{H}-1\right)\right), \tag{37}$$

where μ^* is the magnetic constant in the linear range, $\aleph(x)$ is the Heaviside step function, H_s is the saturation magnetic field.

[2] Note that the constitutive equation for $\mathbf{B}$ may also be written as $\mathbf{H} = \mathbf{B}/\mu_0 - \mathbf{m}$ (Ponte Castañeda and Galipeau, 2011; Galipeau and Ponte Castañeda, 2012), where $\mathbf{m}$ is the Eulerian magnetization. This form of the constitutive equation can be easily recovered by choosing μ to be defined via $\mathbf{m} = (\mu-1)\mathbf{H}$.

ARTICLE IN PRESS

S. Rudykh, K. Bertoldi / J. Mech. Phys. Solids ∎ (∎∎∎∎) ∎∎∎–∎∎∎   7

6.2. Loading conditions

The following macroscopic magneto-mechanical loading conditions are considered:

- *Simple shear in 2D in the presence of a magnetic field* applied in x_2 direction. For this loading case the macroscopic deformation gradient $\overline{\mathbf{F}}$ and the applied magnetic field $\overline{\mathbf{H}}^0$ are given by

$$\overline{\mathbf{F}} = \mathbf{e}_1 \otimes \mathbf{e}_1 + \gamma \mathbf{e}_1 \otimes \mathbf{e}_2 + \mathbf{e}_2 \otimes \mathbf{e}_2 + \mathbf{e}_3 \otimes \mathbf{e}_3 \quad \text{and} \quad \overline{\mathbf{H}}^0 = H_2 \mathbf{e}_2. \tag{44}$$

- *Pure shear in 2D in the presence of a magnetic field* applied in x_2 direction. For this loading case the macroscopic deformation gradient $\overline{\mathbf{F}}$ and the applied magnetic induction $\overline{\mathbf{B}}^0$ are given by

$$\overline{\mathbf{F}} = \lambda \mathbf{e}_1 \otimes \mathbf{e}_1 + \frac{1}{\lambda} \mathbf{e}_2 \otimes \mathbf{e}_2 + \mathbf{e}_3 \otimes \mathbf{e}_3 \quad \text{and} \quad \overline{\mathbf{B}}^0 = B_2 \mathbf{e}_2. \tag{45}$$

- *Axisymmetric shear in 3D in the presence of a magnetic field* applied in x_2 direction. For this loading case the macroscopic deformation gradient $\overline{\mathbf{F}}$ and the applied magnetic induction $\overline{\mathbf{B}}^0$ are given by

$$\overline{\mathbf{F}} = \lambda \mathbf{e}_1 \otimes \mathbf{e}_1 + \lambda^{-2} \mathbf{e}_2 \otimes \mathbf{e}_2 + \lambda \mathbf{e}_3 \otimes \mathbf{e}_3 \quad \text{and} \quad \overline{\mathbf{B}}^0 = B_2 \mathbf{e}_2. \tag{46}$$

Although a generic state of deformation described can be reached by following multiple loading histories, here we focus on the two fundamental non-linear magneto-mechanical paths (see Fig. 3):

- *Path A*: The macroscopic deformation is first applied and then kept constant while increasing the external magnetic field.
- *Path B*: The macroscopic external magnetic field is first applied and then kept constant while increasing the applied deformation.

6.3. Results for simple shear in 2D in the presence of a magnetic field

Motivated by experimental measurement of tangent effective shear moduli of anisotropic MREs (Chen et al., 2003, 2007; Danas et al., 2012), we study simple shear mode of deformations in the presence of a magnetostatic field as specified in (44). We first investigate the onset of instabilities in structures with horizontal and vertical layer orientation, and then we focus on the influence of the lamination angle Θ^0.
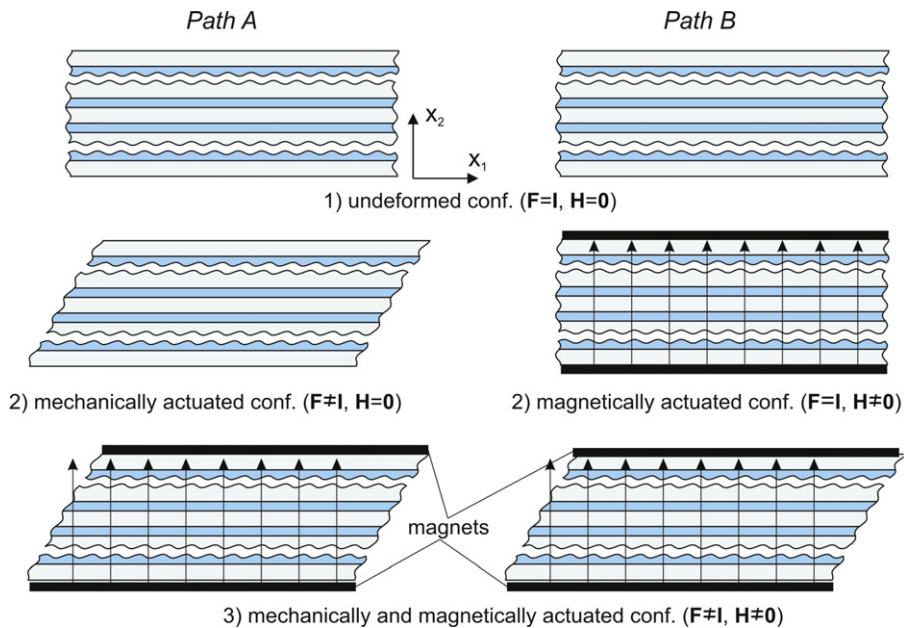

Fig. 3. Schematic representation of the considered loading paths. (For interpretation of the references to color in this figure caption, the reader is referred to the web version of this article.)

ARTICLE IN PRESS

8   *S. Rudykh, K. Bertoldi / J. Mech. Phys. Solids ▮ (▮▮▮▮) ▮▮▮–▮▮▮*

6.3.1. Horizontal layers ($\Theta^0 = 0$)

Macroscopic response: When the magnetic field is normal to the layers (*i.e.*, $\Theta^0 = 0$), the current and Lagrangian magnetic fields are equal (*i.e.*, $\overline{\mathbf{H}} = \overline{\mathbf{H}}^0$) and the Lagrangian magnetic induction is given by

$$\overline{\mathbf{B}}^0 = \check{\mu}H_2(\gamma\overline{\mathbf{e}}_1 + \overline{\mathbf{e}}_2), \tag{47}$$

where $\check{\mu} = (c^{(m)}/\mu^{(m)} + c^{(i)}/\mu^{(i)})^{-1}\mu_0$. It follows that the macroscopic shear stress component $\overline{\sigma}_{12}$ is

$$\overline{\sigma}_{12} = \check{G}\gamma, \tag{48}$$

where $\check{G} = (c^{(m)}/G^{(m)} + c^{(i)}/G^{(i)})^{-1}$. Eq. (48) clearly reveals that the shear stress does not depend on the magnetic field.

Analysis of macroscopic instabilities: Remarkably, for this choice of Θ^0 and loading conditions the onset of macroscopic instabilities (26) takes a compact form

$$\gamma^2 - \left(1 - \frac{\check{\mu}}{\overline{\mu}}\right)\frac{\check{\mu}}{\check{G}}H_2^2 + 1 = 0. \tag{49}$$

Therefore, for *Path A* macroscopic instabilities will occur when

$$\gamma = \left[\left(1 - \frac{\check{\mu}}{\overline{\mu}}\right)\frac{\check{\mu}}{\check{G}}H_2^2 - 1\right]^{1/2}, \tag{50}$$

whereas for *Path B* instability is detected when

$$H_2 = \left[(\gamma^2 + 1)\left(1 - \frac{\check{\mu}}{\overline{\mu}}\right)^{-1}\frac{\check{G}}{\check{\mu}}\right]^{1/2}. \tag{51}$$

Eq. (50) confirms that in the purely mechanical case (*i.e.*, $H_2 = 0$) macroscopic instabilities do not occur (Triantafyllidis et al., 2006; Agoras et al., 2009; Rudykh and deBotton, 2011, 2012). Differently, multilayered MREs characterized by $\Theta^0 = 0$ are found to fail under simple shear in the presence of a magnetic field when conditions (50) and (51) are first met along the loading path.

Fig. 4 shows results for the critical dimensionless magnetic field $H = H_2\sqrt{\mu_0\mu^{(m)}/G^{(m)}}$ at which the macroscopic instabilities develop as a function of the applied shear deformation γ and of the stiff phase volume fraction $c^{(i)}$. It is easy to see that when the material is deformed according to *Path A* larger values of γ stabilize the system. Similarly, for *Path B* larger values of H stabilize the system. Moreover, in both cases larger contrast ratios between the phases result in significant destabilization of MREs.

6.3.2. Vertical layers ($\Theta^0 = \pi/2$)

Next, we consider the case when magnetic field is parallel to the layers (*i.e.*, $\Theta^0 = \pi/2$).

Macroscopic response: In this case, the macroscopic shear stress is given by

$$\overline{\sigma}_{12} = \frac{\gamma}{(1+\gamma^2)^2}[\overline{G}(2+\gamma^2)\gamma^2 + \check{G} + H_2^2(\overline{\mu} - \check{\mu})], \tag{52}$$
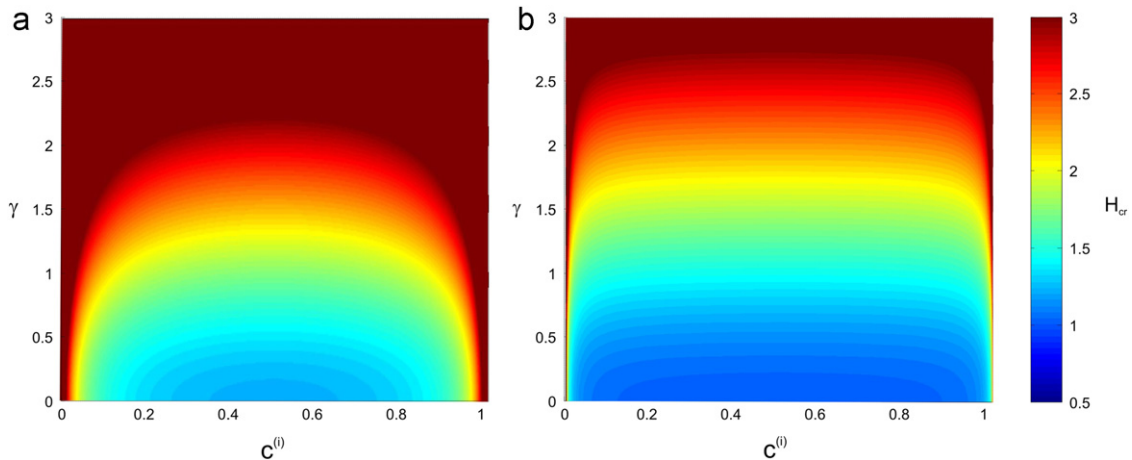

Fig. 4. Simple shear in the presence of a magnetic field: bifurcation diagrams for multilayered MRE with horizontal layers ($\Theta^0 = 0$). The magnitude of the critical magnetic field for the onset of macroscopic instability is shown as a contour map with the adjacent color-bar. The contrast ratio of the phases material constants is $G^{(i)}/G^{(m)} = \mu^{(i)}/\mu^{(m)} = 10$ and 100 in (a) and (b), respectively. (For interpretation of the references to color in this figure caption, the reader is referred to the web version of this article.)
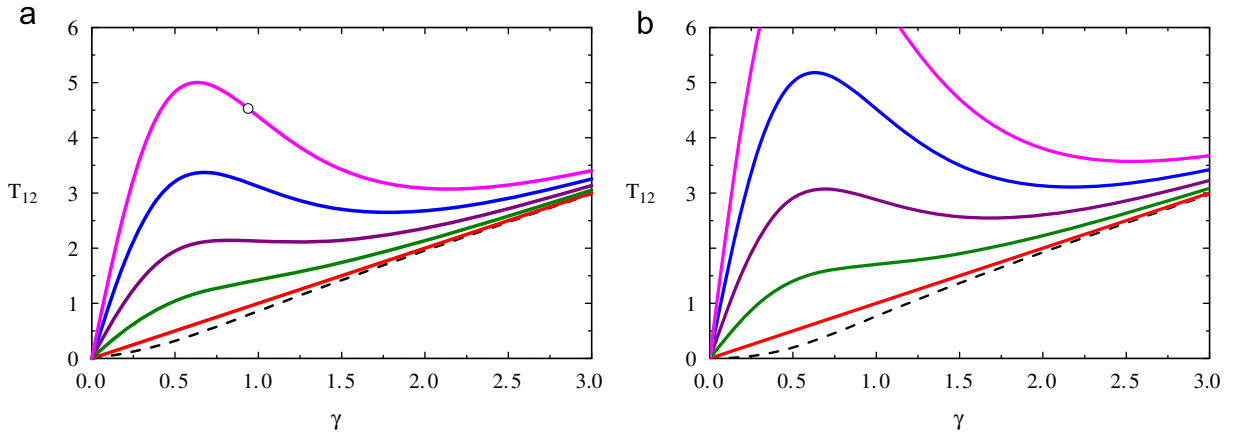
ARTICLE IN PRESS

S. Rudykh, K. Bertoldi / J. Mech. Phys. Solids ▮ (▮▮▮▮) ▮▮▮–▮▮▮   9

Fig. 5. Stress–strain response of anisotropic MREs characterized by $\Theta^0 = \pi/2$ at different levels of the magnetic field H=0.0, 1.0, 2.0, 4.0 and 5.0 (black, red, green, purple, blue and magenta, respectively). The volume fraction of the stiff phase is $c^{(i)} = 0.2$. The contrast ratio of the phases material constants is $G^{(i)}/G^{(m)} = \mu^{(i)}/\mu^{(m)} = 10$ and 100 in (a) and (b), respectively. (For interpretation of the references to color in this figure caption, the reader is referred to the web version of this article.)

where $\overline{G} = G^{(m)}c^{(m)} + G^{(i)}c^{(i)}$. Expression (52) clearly shows the dependence of the shear stress on the magnetic field. Fig. 5 shows the normalized shear stress $T_{12} = \overline{\sigma}_{12}/\overline{G}$ versus γ for composites where the stiffer phase has volume fraction $c^{(i)} = 0.2$. The results corresponding to purely mechanical loading (black dashed curve) are compared to the results of loading in the presence of dimensionless magnetic fields H=1.0, 2.0, 4.0 and 5.0. While for low magnetic fields the stress–strain curves are almost linear, for higher magnetic fields the response is found to be characterized by a prominent local maximum. Therefore for high magnetic fields snap-through instabilities may occur, since small disturbances will lead to sudden jump to the following branch of the equilibrium curve resulting in giant deformations (*e.g.*, Rudykh et al., 2012; Wang et al., 2012; Li et. al., 2013, for snap-through actuation of electroactive media). However, for moderate values of applied deformations (*i.e.*, $|\gamma| \lesssim 0.3$) the response can be approximated by a linear function even for large values of the magnetic field. In particular, Taylor series expansion of the shear stress $\overline{\sigma}_{12}$ (Eq. (52)) around $\gamma = 0$ yields

$$\overline{\sigma}_{12} = [\check{G} + H_2^2(\overline{\mu} - \check{\mu})]\gamma + o(\gamma^3), \tag{53}$$

showing that for moderate γ the shear stress slope monotonically increases as a function of H, leading to larger values of the instantaneous shear modulus. This result nicely agrees with the recent experimental observations, reporting a marked field-induced stiffening in anisotropic MREs (Guan et al., 2008; Danas et al., 2012).

It is also interesting to observe that the curves asymptotically reduce to the one corresponding to the purely mechanical case as the amount of applied shear increases, since the mechanical part of the shear stress becomes dominant over the magnetic stress contribution. Finally, the stress–strain curves clearly show that an increase of the contrast ratios between the layers leads to an increase of the corresponding stress response.

Analysis of macroscopic instabilities: We start by noting that, similar to the previously considered case of $\Theta^0 = 0$, in the purely mechanical case macroscopic instabilities do not occur for $\Theta^0 = \pi/2$. However, when magnetomechanical finite deformations are applied the onset of macroscopic instability can be calculated from Eq. (26). Differently from the case of $\Theta^0 = 0$ here (26) has to be solved numerically, since its roots cannot be obtained explicitly.

In contrast with the case of $\Theta^0 = 0$, here the magnetic field is applied parallel to the layers and acts to stabilize the media. Consequently, in the undeformed configuration ($\gamma = 0$) the composite is stable for any value of H. However, when γ is increased the stability of the system will be determined by the competition between two opposite effects: (i) increasing values of γ will result in a rotation of the layers so that at some critical angle the magnetic field will act to destabilize the material; (ii) increasing values of γ will lead to tension within the layers, and consequently, suppresses instabilities. As a result all the configurations investigated in Fig. 5a and b are stable in the considered range of γ except for the material characterized by $G^{(i)}/G^{(m)} = \mu^{(i)}/\mu^{(m)} = 10$ and subjected to H=5. For this case the onset of macroscopic instability is detected at $\gamma \simeq 0.939$, as marked by a circle in Fig. 5a.

To show a detailed and comprehensive picture illustrating the stability of the considered anisotropic MREs, in Fig. 6 we present results for the critical magnetic field H at which macroscopic instabilities develop as a function of the applied shear deformation γ and of the stiff phase volume fraction $c^{(i)}$. As expected, differently from the case $\Theta^0 = 0$ the material is found to be stable at low values of γ, because of the initially stabilizing role of the magnetic field for this configuration. However, above a critical γ instabilities are observed to occur, facilitated by the inclination of the layers. Interestingly, for large enough amount of applied shear the stabilizing effect of the tension built in the layers dominates, leading to higher values of H. Finally, differently from the case $\Theta^0 = 0$, larger contrast ratios between the phases are observed to stabilize the MREs.

ARTICLE IN PRESS

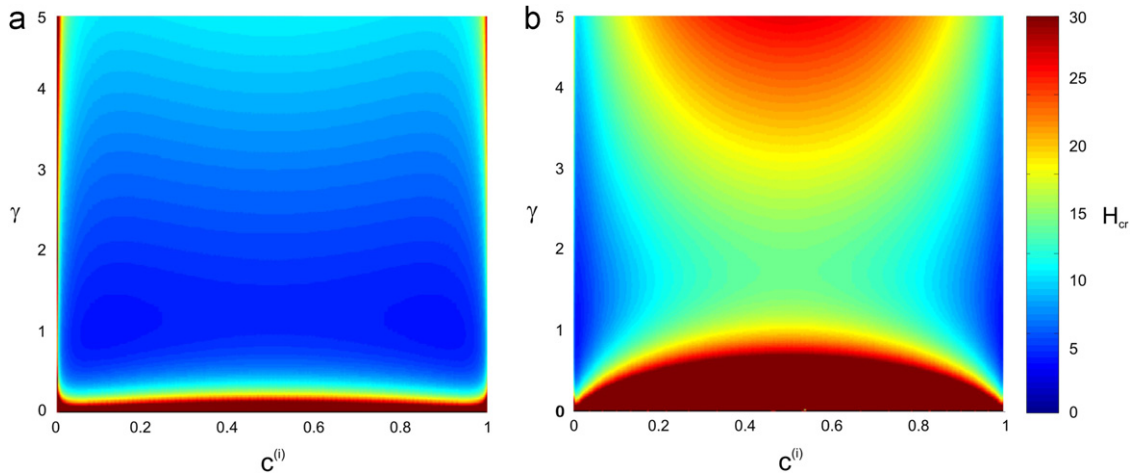10   *S. Rudykh, K. Bertoldi / J. Mech. Phys. Solids ∎ (∎∎∎∎) ∎∎∎–∎∎∎*

Fig. 6. Simple shear in the presence of a magnetic field: bifurcation diagrams for multilayered MRE with vertical layers ($\Theta^0 = \pi/2$). The magnitude of the critical magnetic field for the onset of macroscopic instability is shown as a contour map with the adjacent color-bar. The contrast ratio of the phases material constants is $G^{(i)}/G^{(m)} = \mu^{(i)}/\mu^{(m)} = 10$ and 100 in (a) and (b), respectively. (For interpretation of the references to color in this figure caption, the reader is referred to the web version of this article.)

6.3.3. Influence of the lamination angle Θ^0

Analysis of macroscopic instabilities: Next we analyze the influence of the layers orientation on the macroscopic stability of the composites subjected to simple shear deformation at a magnetic field as specified in (45).

It is well known that for the purely mechanical case multilayered structures may become unstable only when the applied deformation results in compression along the layer direction (*e.g.*,Triantafyllidis and Maker, 1985; Nestorovic and Triantafyllidis, 2004; Agoras et al., 2009; Rudykh and deBotton, 2012). More specifically, under simple shear loading macroscopic instabilities occur when

$$a_4\gamma^4 + a_3\gamma^3 + a_2\gamma^2 + a_1\gamma + a_0 = 0, \tag{54}$$

with

$$a_0 = 8\breve{G}, \quad a_1 = 16\overline{G}\sin 2\Theta^0, \quad a_2 = 4(3\overline{G} + \breve{G} - 2\underline{G}\cos 2\Theta^0 - (\overline{G} - \breve{G})\cos 4\Theta^0),$$

$$a_3 = 4(2\overline{G}\sin 2\Theta^0 + (\breve{G} - \overline{G})\sin 4\Theta^0), \quad a_4 = 3\overline{G} + \breve{G} - 4\underline{G}\cos 2\Theta^0 + (\overline{G} - \breve{G})\cos 4\Theta^0.$$

It can be shown that condition (54) may be eventually satisfied only when $\pi/2 < \Theta^0 < \pi$ (*i.e.*, when the applied deformation results in compression in the layer direction).

The bifurcation diagrams of composites with phase volume fractions $c^{(i)} = 0.2$ are shown in Fig. 7. To highlight the role played by anisotropy the critical levels of magnetic excitation are presented as functions of the lamination angle Θ^0 and the applied amount of shear γ.

We start by noting that purely mechanical instabilities give rise to discontinuities in the critical magnetic field surfaces in the region of $\pi/2 < \Theta^0 < \pi$, as clearly marked in the plot by the while dashed lines corresponding to the onset of macroscopic mechanical instability. We also observe that an increase of contrast ratio in the material properties destabilizes the system when subjected to purely mechanical loading.

By contrast, if the composites are subjected to a magnetomechanical loading, an increase of contrast ratio in the material properties is found to stabilize the system. Moreover, we observe that MREs with low initial lamination angles are less stable systems.

Finally, to highlight the important role played by the magnetic fields for MREs loaded according to *Path A*, in Fig. 8 we plot the critical magnetic field H as a function of Θ^0 at fixed amount of applied shear $\gamma = 0.5$. In the figure the light and dark shadowed regions correspond to the stable and unstable domains, respectively. We observe that when there is no magnetic field applied (*i.e.*, $H=0$), MREs characterized by $G^{(i)}/G^{(m)} = \mu^{(i)}/\mu^{(m)} = 10$ and 100 are unstable for $0.681 < \Theta^0 < 0.897\pi$ and $0.591 < \Theta^0 < 0.987\pi$, respectively (see Fig. 8a and b). Remarkably, we observe that a relatively low applied magnetic fields H is capable of significant stabilization. For example at $\Theta^0 = 0.7\pi$ and $H=0$ both MREs investigated in Fig. 8 are unstable, however they become stable when a magnetic field $H=0.4$ and 0.9 is applied for $G^{(i)}/G^{(m)} = \mu^{(i)}/\mu^{(m)} = 10$ and 100, respectively.
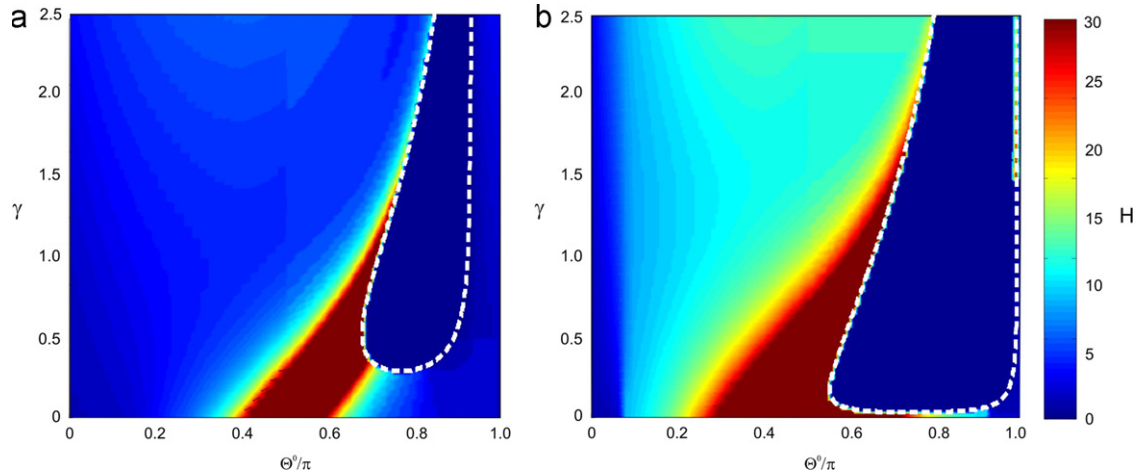
ARTICLE IN PRESS

S. Rudykh, K. Bertoldi / J. Mech. Phys. Solids ▮ (▮▮▮▮) ▮▮▮–▮▮▮　　11

Fig. 7. Simple shear in the presence of a magnetic field: bifurcation diagrams for multilayered MRE with varying orientation of layers. The magnitude of the critical magnetic field for the onset of macroscopic instability is shown as a contour map with the adjacent color-bar. The contrast ratio of the phases material constants is $G^{(i)}/G^{(m)} = \mu^{(i)}/\mu^{(m)} = 10$ and 100 in (a) and (b), respectively. The volume fraction of the stiff phase is $c^{(i)} = 0.2$. The white dashed curves correspond to the onset of macroscopic instability for the purely mechanical case. (For interpretation of the references to color in this figure caption, the reader is referred to the web version of this article.)
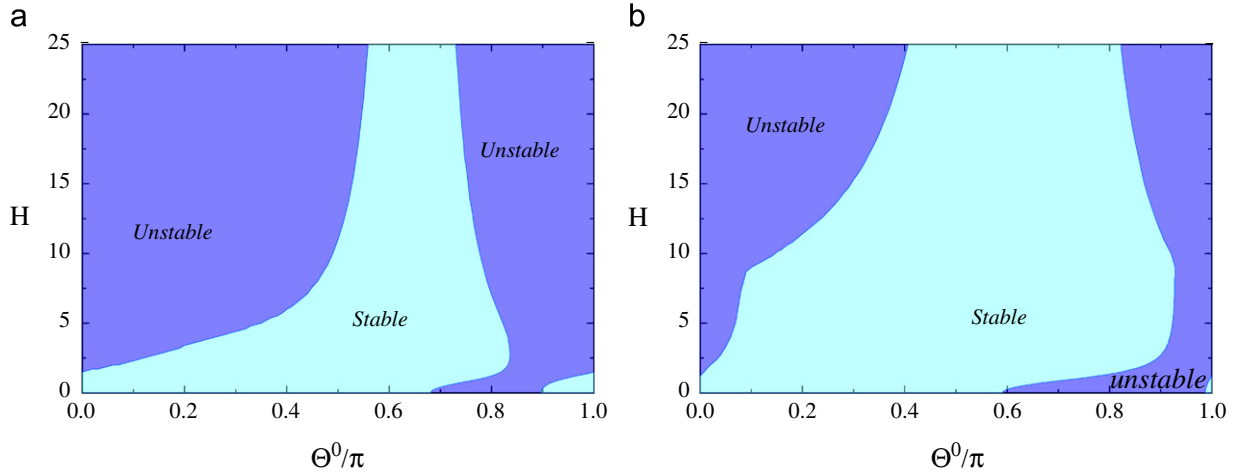

Fig. 8. Simple shear in the presence of a magnetic field: bifurcation diagrams for multilayered MRE varying orientation of layers. The magnitude of the critical magnetic field for the onset of macroscopic instability is shown as a function of Θ^0 at fixed $\gamma = 0.5$. The contrast ratio of the phases material constants is $G^{(i)}/G^{(m)} = \mu^{(i)}/\mu^{(m)} = 10$ and 100 in (a) and (b), respectively. (For interpretation of the references to color in this figure caption, the reader is referred to the web version of this article.)

6.4. Results for pure shear in 2D in the presence of magnetic field

In this section we investigate pure shear mode of deformations in the presence of a magnetic field. As for the case of simple shear, we first investigate the onset of instabilities in structures with horizontal and vertical layer orientation, and then focus on the influence of the lamination angle Θ^0.

6.4.1. Horizontal layers ($\Theta^0 = 0$)

Macroscopic response: For MREs with horizontal layers (*i.e.*, $\Theta^0 = 0$) the only non-zero component of the Lagrangian magnetic field is

$$H_2^0 = \frac{B_2^0}{\bar{\mu}\bar{\lambda}^2} \tag{55}$$

so that

$$T = \frac{(\bar{\sigma}_{11} - \bar{\sigma}_{22})}{\bar{G}} = \lambda^2 - \left(\frac{B_2^2}{\bar{\mu}\bar{G}} + 1\right)\lambda^{-2}. \tag{56}$$

ARTICLE IN PRESS

12   S. Rudykh, K. Bertoldi / J. Mech. Phys. Solids ▮ (▮▮▮▮) ▮▮▮–▮▮▮
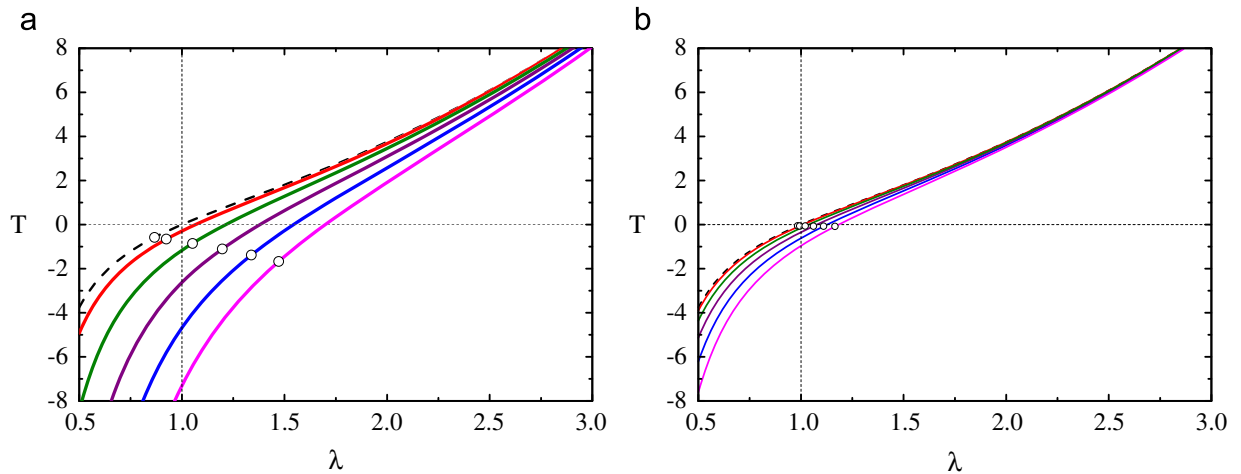
Fig. 9. Stress–strain response of anisotropic MREs characterized by $\Theta^0 = 0$ at different levels of the magnetic excitation $B=0.0, 1.0, 2.0, 4.0$ and 5.0 (black, red, green, purple, blue, and magenta curves, respectively). The volume fraction of the stiffer phase is $c^{(i)} = 0.2$. The phase material constant contrast ratios are $G^{(i)}/G^{(m)} = \mu^{(i)}/\mu^{(m)} = 10$ and 100 in pictures (a) and (b), respectively. (For interpretation of the references to color in this figure caption, the reader is referred to the web version of this article.)

Fig. 9 shows the evolution of the normalized stress T as the function of the applied stretch λ for composites with $c^{(i)} = 0.2$. The purely mechanical response is compared to that of composites in the presence of increasing levels of dimensionless magnetic induction $B = B_2/\sqrt{G^{(m)}\mu^{(m)}\mu_0} = 1.0, 2.0, 4.0$ and 5.0.

Clearly, under tension (*i.e.*, $\lambda > 1$) the magnetic field reduces the stress level in the material, so that the highest curve is the one corresponding to the purely mechanical case. However, at relatively high values of the applied stretch the contribution of the magnetostatic stresses decreases and the purely mechanical part of the total stress becomes dominant, so that the curves of the magnetically excited materials approach the purely mechanical ones. By contrast, in compression (*i.e.*, $\lambda < 1$) the magnetic field is found to increase the stress level in the material and its contribution becomes more pronounced for large values of the applied deformation. Finally, we observe that increasing the contrast ratios of the material properties the mechanical stress contribution becomes dominant, so that all the curves approach that corresponding to the purely mechanical loading.

Analysis of macroscopic instabilities: Remarkably, for $\Theta^0 = n\pi$ and $\Theta^0 = \pi/2 + n\pi$ with $n = 0,1,2\ldots$, the coefficients Γ_1, Γ_3, Γ_5 in Eq. (26) vanish and the criterion for the onset of instabilities can be written as a bi-cubic polynomial

$$\Gamma_6\xi^6 + \Gamma_4\xi^4 + \Gamma_2\xi^2 + \Gamma_0 = 0. \tag{57}$$

More specifically, when the material is loaded according to *Path A* the onset of macroscopic instability is detected when

$$\lambda = \left[1 - \frac{\check{G}}{\bar{\bar{G}}} + \frac{B_2^2}{\bar{G}\check{\mu}}\left(1 - \frac{\check{\mu}}{\bar{\mu}}\right)\right]^{1/4}, \tag{58}$$

whereas for *Path B* instability will occur when

$$B_2 = \left[\left(\lambda^4 - 1 + \frac{\check{G}}{\bar{\bar{G}}}\right)\left(1 - \frac{\check{\mu}}{\bar{\mu}}\right)^{-1}\check{\mu}\bar{G}\right]^{1/2}. \tag{59}$$

Therefore for the purely mechanical case (*i.e.*, $B_2 = 0$), as predicted by Triantafyllidis and Maker (1985), an increase of the contrast ratio of the constituents material reduces the stable domain and for the two limiting cases $c^{(i)} \to 0$ and $c^{(m)} \to 0$ the material is observed to be stable.

Fig. 10 shows the bifurcation diagrams, reporting the dimensionless critical magnetic field B as a function of the applied stretch λ and of the volume fraction of the stiffer magnetoactive phase. The white dashed curves in the plots correspond to the onset of macroscopic instability for the purely mechanical case.

Differently from the purely mechanical case where the bifurcation diagrams are symmetric with respect to $c^{(i)} = 0.5$, in the presence of a magnetic field composites with low volume fractions of the stiffer phase (*i.e.*, $c^{(i)} \to 0$) are less stable than those with higher concentration of the stiff phase (*i.e.*, $c^{(i)} \to 1$). Moreover, increasing values of both applied deformation λ and phases material contrasts are found to stabilize the system. Interestingly, for high contrast ratios of the phase material

ARTICLE IN PRESS

S. Rudykh, K. Bertoldi / J. Mech. Phys. Solids ∎ (∎∎∎∎) ∎∎∎–∎∎∎   13
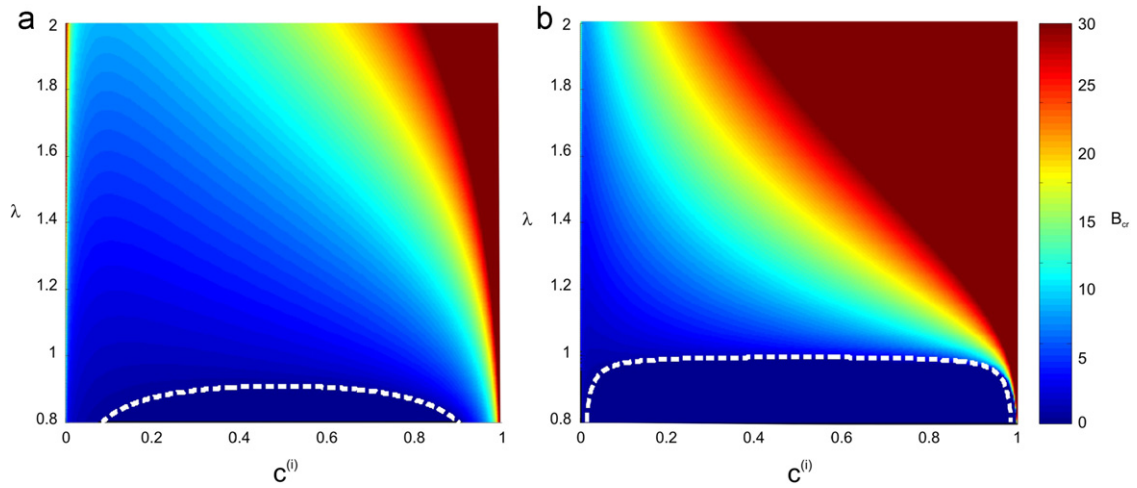

Fig. 10. Pure shear in the presence of a magnetic field: bifurcation diagrams for multilayered MRE with horizontal layers ($\Theta^0 = 0$). The magnitude of the critical magnetic field for the onset of macroscopic instability is shown as a contour map with the adjacent color-bar. The contrast ratio of the phases material constants is $G^{(i)}/G^{(m)} = \mu^{(i)}/\mu^{(m)} = 10$ and 100 in (a) and (b), respectively. The white dashed curves correspond to the onset of macroscopic instability for the purely mechanical case. (For interpretation of the references to color in this figure caption, the reader is referred to the web version of this article.)

constants the composite becomes extremely unstable when $c^{(i)} \to 0$, while in the limit of dilute soft magnetoactive phase the stability of the composites is not significantly influenced by magnetic excitation.

6.4.2. Vertical layers ($\Theta^0 = \pi/2$)
   Macroscopic response: When $\Theta^0 = \pi/2$, the only non-zero component of the Lagrangian magnetic field is

$$H_2^0 = \frac{B_2^0}{\overline{\mu}\lambda^2} \tag{60}$$

so that the dimensionless stress T is given by

$$T = \lambda^2 - \left(\frac{B_2^2}{\overline{G}\overline{\mu}} + 1\right)\lambda^{-2}. \tag{61}$$

   Fig. 11 reports the evolution of T as a function of the applied stretch λ for composites with $c^{(i)} = 0.2$ and contrast ratios $G^{(i)}/G^{(m)} = \mu^{(i)}/\mu^{(m)} = 10$ and 100 in (a) and (b), respectively. The black dashed curves correspond to the purely mechanical loading, while the red, green, purple, blue and magenta curves correspond to the response in the presence of magnetic fields $B = 1.0, 2.0, 4.0$ and 5.0, respectively. Although the stress–strain behavior is similar to that obtained for the case $\Theta^0 = 0$, in this case the purely mechanical stresses become dominant over the magnetostatic ones much quicker for the increasing values of contrast ratio, as can be easily seen in Fig. 11b where all the curves overlap.
   Analysis of macroscopic instabilities: For the case considered here (*i.e.*, $\Theta^0 = \pi/2$), the bifurcation points for *Path A* can be identified by

$$\lambda = \left(1 - \frac{\check{G}}{\overline{\overline{G}}}\right)^{-1/4}\left[1 + \frac{B_2^2}{\overline{G}\overline{\mu}}\left(1 - \frac{\check{\mu}}{\overline{\mu}}\right)\right]^{1/4}, \tag{62}$$

which stems from (26) and appropriately reduces to the well-known result of Triantafyllidis and Maker (1985) for the purely mechanical case ($B = 0$). In Fig. 11 the onsets of bifurcations are denoted by circles and occur in tension, since $\lambda > 1$ results in compression in the layer direction.
   Moreover, for *Path B* the critical magnetic excitation can be easily obtained from (62) as

$$B_2 = \left\{\left[\lambda^4\left(1 - \frac{\check{G}}{\overline{\overline{G}}}\right) - 1\right]\left(1 - \frac{\check{\mu}}{\overline{\mu}}\right)^{-1}\overline{\mu}\overline{G}\right\}^{1/2}. \tag{63}$$

Fig. 12 shows the dimensionless critical magnetic excitation B as a function of the stretch measured in the layer direction λ^{-1} and of the volume fraction of the stiffer magnetoactive phase. First, we observe that for small values of compressive stretch in the layer direction (*i.e.*, $\lambda^{-1} \sim 1$) the material is stable, as indicated by the white blank region in the figures, and that the stable domain is separated from the unstable domains by a failure surface corresponding to the purely mechanical case, namely $B = 0$.
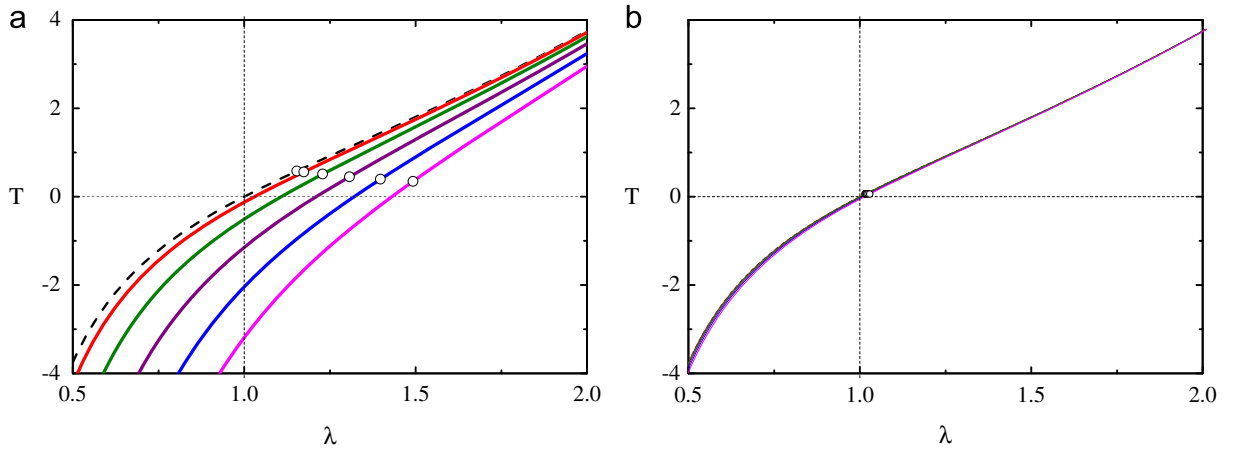
ARTICLE IN PRESS

14   S. Rudykh, K. Bertoldi / J. Mech. Phys. Solids ∎ (∎∎∎∎) ∎∎∎–∎∎∎

Fig. 11. The dependance of the stress on the stretch ratio for the anisotropic MRE with $\Theta^0 = \pi/2$ (the layers are aligned with the magnetic field and normal to the stretch direction) at different levels of the magnetic field $B = 0.0$, 1.0, 2.0, 4.0 and 5.0. (black, red, green, purple, blue, and magenta, respectively). The volume fraction of the stiff phase is $c^{(i)} = 0.2$. The phase material constant contrast ratios are $G^{(i)}/G^{(m)} = \mu^{(i)}/\mu^{(m)} = 10$ and 100 in pictures (a) and (b), respectively. (For interpretation of the references to color in this figure caption, the reader is referred to the web version of this article.)
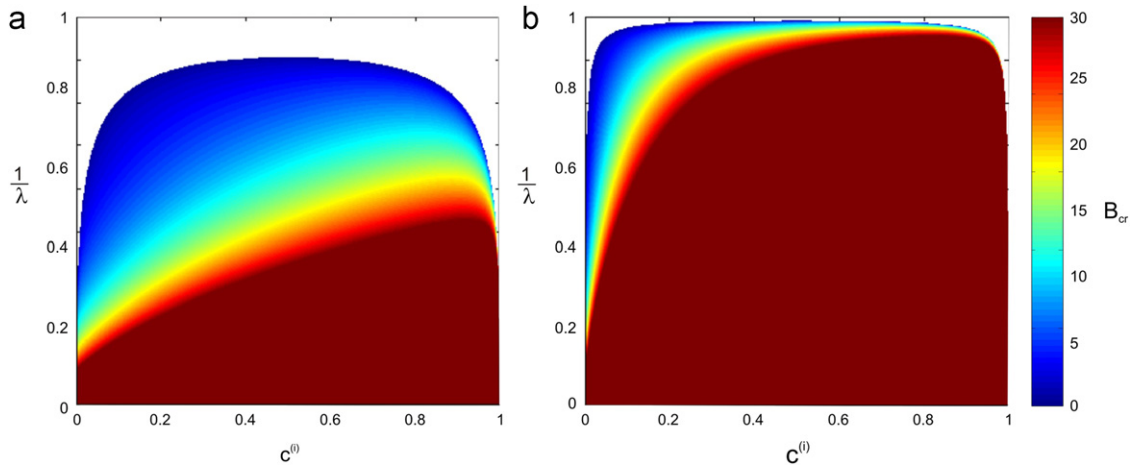

Fig. 12. Pure shear in the presence of a magnetic field: bifurcation diagrams for multilayered MRE with vertical layers. The magnitude of the critical magnetic field for the onset of macroscopic instability is shown as a contour map with the adjacent color-bar. The contrast ratio of the phases material constants is $G^{(i)}/G^{(m)} = \mu^{(i)}/\mu^{(m)} = 10$ and 100 in (a) and (b), respectively. (For interpretation of the references to color in this figure caption, the reader is referred to the web version of this article.)

It is easy to see that here the magnetic field stabilizes the material, since higher applied magnetic fields result in higher compressive stretches needed to achieve instabilities. Moreover, we note that the stabilizing effect of the applied magnetic field is more significant in the range of low volume fractions of the magnetoactive inclusions (i.e., $c^{(i)} < 0.5$). Finally, larger contrast ratios between the phases are observed to destabilize the MREs.

6.4.3. Influence of the lamination angle Θ^0

Analysis of macroscopic instabilities: To highlight the effect of material anisotropy on the material stability we now investigate the influence of the lamination angle Θ^0. For the purely mechanical loading it has been shown (Agoras et al., 2009) that a macroscopic instability occurs when

$$\lambda^8 \cos^2\Theta^0 [\overline{G} + \check{G} + (\overline{G} - \check{G})\cos 2\Theta^0] - \lambda^4 \frac{\overline{G} - \check{G}}{2}(3 + \cos 4\Theta^0) + [\overline{G} + \check{G} - (\overline{G} + \check{G})\cos 2\Theta^0]\sin^2\Theta^0 = 0. \quad (64)$$

It can be shown that Eq. (64) admits a real solution λ only when the applied mechanical deformation results in compression in the layer direction. For the case of pure shear loading considered here this occurs only when $\Theta < \pi/4$ (Rudykh and de Botton, 2012), deBotton with $\Theta = \arctan(\lambda^2 \tan\Theta^0)$ denoting the lamination angle in the deformed configuration.
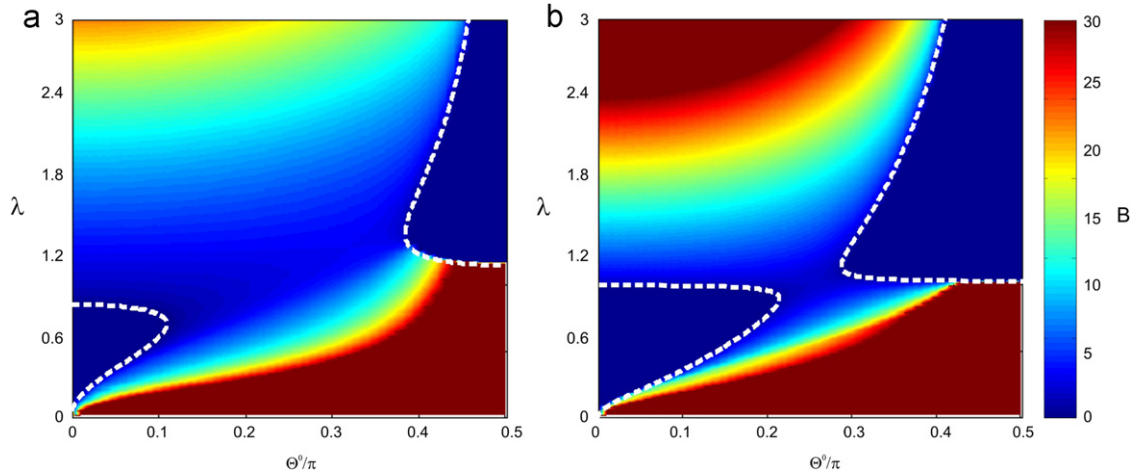
ARTICLE IN PRESS

S. Rudykh, K. Bertoldi / J. Mech. Phys. Solids ▮ (▮▮▮▮) ▮▮▮–▮▮▮   15

Fig. 13. Pure shear in the presence of a magnetic field: bifurcation diagrams for multilayered MRE with varying orientation of the layers. The magnitude of the critical magnetic field for the onset of macroscopic instability is shown as a contour map with the adjacent color-bar. The volume fraction of the stiffer phase is $c^{(i)} = 0.2$. The contrast ratio of the phases material constants is $G^{(i)}/G^{(m)} = \mu^{(i)}/\mu^{(m)} = 10$ and 100 in (a) and (b), respectively. The volume fraction of the stiff phase is $c^{(i)} = 0.2$. The white dashed curves correspond to the onset of macroscopic instability for the purely mechanical case. (For interpretation of the references to color in this figure caption, the reader is referred to the web version of this article.)

The bifurcation diagrams for coupled magnetomechanical loadings of composites with phase volume fractions $c^{(i)} = 0.2$ are shown in Fig. 13. To highlight the role of the anisotropy, the critical levels of magnetic excitation B are presented as functions of the lamination angle Θ^0 and stretch ratio λ.

In both plots we can observe purely mechanical unstable domains, highlighted by the white dashed curves. As expected, an increase of the contrast ratio leads to the expansions of these domains.

In contrast to the purely mechanical case, under coupled magnetomechanical loadings instabilities may develop in composites with lamination angles beyond $\Theta = \pi/4$. Focusing on the bottom part of the plots which corresponds to compression (i.e., $\lambda < 1$) we observe that an increase of the lamination angle Θ^0 results in stabilization of the material and, consequently, in higher values of the critical level of magnetic excitation. Differently, when a tensile deformation (i.e., $\lambda > 1$) is applied to the MRE an increase of Θ^0 is found to destabilize the composite, leading to lower values of the critical magnetic excitation. We also note that the switch in the role of the lamination angle Θ^0 happens near $\lambda \approx 1$, but its exact location depends on the material properties.

6.5. Results for axisymmetric shear in 3D in the presence of magnetic field

Finally, we investigate a 3D mode of deformations in the presence of a magnetostatic field as specified in (46), considering multilayers characterized by $\Theta^0 = 0$.

Macroscopic response: For MREs with $\Theta^0 = 0$ the only non-zero component of the magnetic field vector is

$$H_2 = \frac{B_2}{\check{\mu}\lambda^4}, \tag{65}$$

so that

$$T = \frac{(\overline{\sigma}_{11} - \overline{\sigma}_{22})}{\overline{G}} = \lambda^2 - \left(\frac{B_2^2}{\check{\mu}\overline{G}} + 1\right)\lambda^{-4}, \tag{66}$$

with $\sigma_{11} = \sigma_{33} = \overline{G}\lambda^2 - p$.

The evolution of the normalized stress T as a function of the applied stretch λ for composites with $c^{(i)} = 0.2$ is reported in Fig. 14, where the purely mechanical response is compared to that of composites in the presence of increasing levels of dimensionless magnetic induction $B = B_2/\sqrt{G^{(m)}\mu^{(m)}\mu_0} = 1.0$, 2.0, 4.0 and 5.0. As expected, the stress–strain response shows the same features previously observed for pure shear in 2D with $\Theta^0 = 0$ (see Section 6.4.1).

Analysis of macroscopic instabilities: Making use of Eq. (23), for *Path A* the onset of macroscopic instability is detected when

$$\lambda = \left(1 - \frac{\check{G}}{\overline{G}} + \frac{B_2^2}{\check{\mu}\overline{G}}\right)^{1/6}, \tag{67}$$

ARTICLE IN PRESS

18   S. Rudykh, K. Bertoldi / J. Mech. Phys. Solids ∎ (∎∎∎∎) ∎∎∎–∎∎∎

Finally, defining $\xi = a_2/a_1$, Eq. (A.2) can be rewritten as

$$
\begin{aligned}
&-(\mathcal{M}_{122}-(\mathcal{M}_{112}+\mathcal{M}_{121}-\mathcal{M}_{222})\xi-(\mathcal{M}_{122}+\mathcal{M}_{221}-\mathcal{M}_{111})\xi^2+\mathcal{M}_{121}\xi^3)^2+(\mathcal{A}_{2121}+\xi[2\mathcal{A}_{2122}-2\mathcal{A}_{1121}\\
&\quad+\xi(\mathcal{A}_{1111}-2\mathcal{A}_{1122}-2\mathcal{A}_{1221}+\mathcal{A}_{2222}+\xi(2\mathcal{A}_{1112}-2\mathcal{A}_{1222}+\mathcal{A}_{1212}\xi))])(\mathcal{H}_{22}+\xi(\mathcal{H}_{11}\xi-2\mathcal{H}_{12}))\\
&=0,
\end{aligned}
\tag{A.3}
$$

that can be reorganized in the form of a sextic polynomial as in Eq. (26) with the coefficients Γ_i is given by

$$\Gamma_0 = \mathcal{M}_{122}^2 - \mathcal{A}_{2121}\mathcal{H}_{22},$$

$$\Gamma_1 = 2(\mathcal{A}_{2121}\mathcal{H}_{12}+(\mathcal{A}_{1121}-\mathcal{A}_{2122})\mathcal{H}_{22}-\mathcal{M}_{122}(\mathcal{M}_{112}+\mathcal{M}_{121}-\mathcal{M}_{222})),$$

$$
\begin{aligned}
\Gamma_2 &= -\mathcal{A}_{2121}\mathcal{H}_{11}-4(\mathcal{A}_{1121}-\mathcal{A}_{2122})\mathcal{H}_{12}-(\mathcal{A}_{1111}-2\mathcal{A}_{1122}-2\mathcal{A}_{1221}+\mathcal{A}_{2222})\mathcal{H}_{22}\\
&\quad+2\mathcal{M}_{122}(\mathcal{M}_{111}-\mathcal{M}_{122}-\mathcal{M}_{221})+(\mathcal{M}_{112}+\mathcal{M}_{121}-\mathcal{M}_{222})^2,
\end{aligned}
$$

$$
\begin{aligned}
\Gamma_3 &= 2((\mathcal{A}_{1121}-\mathcal{A}_{2122})\mathcal{H}_{11}+(\mathcal{A}_{1111}-2\mathcal{A}_{1122}-2\mathcal{A}_{1221}+\mathcal{A}_{2222})\mathcal{H}_{12}\\
&\quad+(\mathcal{A}_{1222}-\mathcal{A}_{1112})\mathcal{H}_{22}+(\mathcal{M}_{121}\mathcal{M}_{122}-(\mathcal{M}_{111}-\mathcal{M}_{122}-\mathcal{M}_{221})(\mathcal{M}_{112}+\mathcal{M}_{121}-\mathcal{M}_{222}))),
\end{aligned}
$$

$$
\begin{aligned}
\Gamma_4 &= -(\mathcal{A}_{1111}-2\mathcal{A}_{1122}-2\mathcal{A}_{1221}+\mathcal{A}_{2222})\mathcal{H}_{11}+4(\mathcal{A}_{1112}-\mathcal{A}_{1222})\mathcal{H}_{12}\\
&\quad-\mathcal{A}_{1212}\mathcal{H}_{22}+(\mathcal{M}_{122}+\mathcal{M}_{221}-\mathcal{M}_{111})^2-2\mathcal{M}_{121}(\mathcal{M}_{112}+\mathcal{M}_{121}-\mathcal{M}_{222}),
\end{aligned}
$$

$$\Gamma_5 = 2((\mathcal{A}_{1222}-\mathcal{A}_{1112})\mathcal{H}_{11}+\mathcal{A}_{1212}\mathcal{H}_{12}+\mathcal{M}_{121}(\mathcal{M}_{111}-\mathcal{M}_{122}-\mathcal{M}_{221})),$$

$$\Gamma_6 = \mathcal{M}_{121}^2 - \mathcal{A}_{1212}\mathcal{H}_{11}. \tag{A.4}$$

References

Agoras, M., Lopez-Pamies, O., Ponte Castañeda, P., 2009. Onset of macroscopic instabilities in fiber-reinforced elastomers at finite strain. J. Mech. Phys. Solids 57, 1828–1850.

Bertoldi, K., Boyce, M.C., 2008. Wave propagation and instabilities in monolithic and periodically structured elastomeric materials undergoing large deformations. Phys. Rev. B 78, 184107.

Bertoldi, K., Gei, M., 2011. Instabilities in multilayered soft dielectrics. J. Mech. Phys. Solids 59, 18–42.

Biot, M.A., 1965. Mechanics of Incremental Deformations. John Wiley and Sons, New-York.

Brigadnov, I.A., Dorfmann, A., 2003. Mathematical modeling of magneto-sensitive elastomers. Int. J. Solids Struct. 40, 4659–4674.

Bruno, D., Greco, F., Lonetti, P., Blasi, P.N., Sgambitterra, G., 2010. An investigation on microscopic and macroscopic stability phenomena of composite solids with periodic microstructure. Int. J. Solids Struct. 47 (20), 2806–2824.

Bustamante, R., 2010. Transversely isotropic nonlinear magneto-active elastomers. Acta Mech. 210, 183–214.

Bustamante, R., Dorfmann, A., Ogden, R., 2006. Universal relations in isotropic nonlinear magnetoelasticity. Q. J. Mech. Appl. Math. 59, 435–450.

Chen, L., Gong, X.L., Li, W.H., 2007. Microstructures and viscoelastic properties of anisotropic magnetorheological elastomers. Smart Mater. Struct. 16, 2645–2650.

Chen, T., Nan, C.-W., Weng, G.J., 2003. Exact connections between effective magnetostriction and effective elastic moduli of fibrous composites and polycrystals. J. Appl. Phys. 94, 491–495.

Danas, K., Kankanala, S.V., Triantafyllidis, N., 2012. Experiments and modeling of iron-particle-filled magnetorheological elastomers. J. Mech. Phys. Solids 60, 120–138.

deBotton, G., 2005. Transversely isotropic sequentially laminated composites in finite elasticity. J. Mech. Phys. Solids 53, 1334–1361.

Deng, H., Gong, X., Wang, L., 2006. Development of an adaptive tuned vibration absorber with magnetorheological elastomer. Smart Mater. Struct. 15, N111–N116.

Destrade, M., Ogden, R.W., 2011. On magneto-acoustic waves in finitely deformed elastic solids. Math. Mech. Solids 16, 594–604.

Dorfmann, A., Ogden, R.W., 2004. Nonlinear magnetoelastic deformations. Q. J. Mech. Appl. Math. 57, 599–622.

Dorfmann, A., Ogden, R.W., 2005. Some problems in nonlinear magnetoelasticity. Z. Angew. Math. Phys. 56, 718–745.

Dorfmann, A., Ogden, R.W., 2010. Nonlinear electroelastostatics: incremental equations and stability. Int. J. Eng. Sci. 48, 1–14.

Farshad, M., Benine, A., 2004. Magnetoactive elastomer composites. Polym Test 23, 347–353.

Farshad, M., Le Roux, M., 2004. A new active noise abatement barrier system. Polym Test 23, 855–860.

Fleck, N., 1997. Compressive failure of fiber composites. Adv. Appl. Mech. 33, 43–117.

Galipeau, E., Ponte Castañeda, P., 2012. The effect of particle shape and distribution on the macroscopic behavior of magnetoelastic composites. Int. J. Solids Struct. 49, 1–17.

Galipeau, E., Rudykh, S., deBotton, G., Ponte Castañeda, P., Magnetorheological elastomers with periodic and random microstructures. Int. J. Solids Struct.(forthcoming).

Geymonat, G., Müller, S., Triantafyllidis, N., 1993. Homogenization of nonlinearly elastic materials, microscopic bifurcation and macroscopic loss of rank-one convexity. Arch. Ration. Mech. Anal. 122, 231–290.

Ginder, J.M., Clark, S.M., Schlotter, W.F., E., N.M., 2002. Magnetostrictive phenomena in magnetorheological elastomers. Int. J. Mod. Phys. B, 16, 2412–2418.

Ginder, J.M., Nichols, M.E., Elie, L.D., Clark, S.M., 2000. Controllable-stiffness components based on magnetorheological elastomers. Proc. SPIE 3985, 418.

Ginder, J.M., Schlotter, W.F., Nichols, M.E., 2001. Magnetorheological elastomers in tunable vibration absorbers. Proc. SPIE 4331, 103.

Gong, X.L., Zhang, X.Z., Zhang, P.Q., 2005. Fabrication and characterization of isotropic magnetorheological elastomers. Polym Test 24 (5), 669–676.

Guan, X., Donga, X., Ou, J., 2008. Magnetostrictive effect of magnetorheological elastomer. J. Magn. Magn. Mater. 320, 158–163.

Han, Y., Zhang, Z., Faidley, L., Hong, W., 2012. Microstructure-based modeling of magneto-rheological elastomers. In: Goulbourne, N., Ounaies, Z. (Eds.), Behavior and Mechanics of Multifunctional Materials and Composites, 2012, vol. 8342. . Proceedings of the SPIE, San Diego, CA, pp. 83421B.

Hill, R., 1957. On uniqueness and stability in the theory of finite elastic strain. J. Mech. Phys. Solids 5, 229–241.

Hill, R., Hutchinson, J.W., 1975. Bifurcation phenomena in the plane tension test. J. Mech. Phys. Solids 23, 239–264.

Hoang, N., Zhang, N., Du, H., 2011. An adaptive tunable vibration absorber using a new magnetorheological elastomer for vehicular powertrain transient vibration reduction. Smart Mater. Struct. 20, 015019.

Jolly, M.R., Carlson, J.D., Munoz, B.C., 1996. A model of the behaviour of magnetorheological materials. Smart Mater. Struct. 5, 607–614.

ARTICLE IN PRESS

S. Rudykh, K. Bertoldi / J. Mech. Phys. Solids ∎ (∎∎∎∎) ∎∎∎–∎∎∎   19

Kankanala, S.V., Triantafyllidis, N., 2008. Magnetoelastic buckling of a rectangular block in plane strain. J. Mech. Phys. Solids 56, 1147–1169.

Li, T., Keplinger, C., Baumgartner, R., Bauer, S., Yang, W., Suo, Z., 2013. Giant voltage-induced deformation in dielectric elastomers near the verge of snap-through instability. J. Mech. Phys. Solids 61, 611–628.

Lerner, A.A., Cunefare, K.A., 2008. Performance of MRE-based vibration absorbers. J. Intell. Mater. Syst. Struct. 19, 551–563.

Maugin, G.A., Eringen, A.C., 1972. Deformable magnetically saturated media, I. Field equations. J. Math. Phys. 13, 143–155.

Michel, J.C., Lopez-Pamies, O., Castañeda, P.P., Triantafyllidis, N., 2007. Microscopic and macroscopic instabilities in finitely strained porous elastomers. J. Mech. Phys. Solids 55, 900–938.

Nestorovic, M.D., Triantafyllidis, N., 2004. Onset of failure in finitely strained layered composites subjected to combined normal and shear loading. J. Mech. Phys. Solids 52, 941–974.

Otténio, M., Destrade, M., Ogden, R., 2008. Incremental magnetoelastic deformations, with application to surface instability. J. Elasticity 90, 19–42.

Ponte Castañeda, P., Galipeau, E., 2011. Homogenization-based constitutive models for magnetorheological elastomers at finite strain. J. Mech. Phys. Solids 59, 194–215.

Rudykh, S., Bhattacharya, K., deBotton, G., 2012. Snap-through actuation of thick-wall electroactive balloons. Int. J. Nonlinear Mech. 47, 206–209.

Rudykh, S., deBotton, G., 2011. Stability of anisotropic electroactive polymers with application to layered media. Z. Angew. Math. Phys. 62, 1131–1142.

Rudykh, S., deBotton, G., 2012. Instabilities of hyperelastic fiber composites: micromechanical versus numerical analyses. J. Elasticity 106, 123–147.

Thylander, S., Menzel, A., Ristinmaa, M., 2012. An electromechanically coupled micro-sphere framework: application to the finite element analysis of electrostrictive polymers. Smart Mater. Struct. 21 (9).

Tian, T.F., Li, W.H., Deng, Y.M., 2011. Sensing capabilities of graphite based MR elastomers. Smart Mater. Struct. 20, 025022.

Tiersten, H., 1964. Coupled magnetomechanical equations for magnetically saturated insulators. J. Math. Phys. 5 (9), 1298–1318.

Tiersten, H., 1965. Variational principle for saturated magnetoelastic insulators. J. Math. Phys. 6 (5), 779–787.

Triantafyllidis, N., Maker, B.N., 1985. On the comparison between microscopic and macroscopic instability mechanisms in a class of fiber-reinforced composites. J. Appl. Mech. Trans. ASME 52, 794–800.

Triantafyllidis, N., Nestorovic, M.D., Schraad, M.W., 2006. Failure surfaces for finitely strained two-phase periodic solids under general in-plane loading. J. Appl. Mech. Trans. ASME 73 (3), 505–515.

Truesdell, C., Toupin, R., 1960. The classical field theories. In: Handbuch der Physik, vol. III. Springer, Berlin.

Varga, Z., Filipcsei, G., Zrinyi, M., 2006. Magnetic field sensitive functional elastomers with tuneable elastic modulus. Polymer 47 (1), 227–233.

Wang, H., Cai, S., Carpi, F., Suo, Z., 2012. Computational model of hydrostatically coupled dielectric elastomer actuators. J. Appl. Mech. Trans. ASME 79 (3).

Zadov, B., Elmalem, A., Paperno, E., Gluzman, I., Nudelman, A., Levron, D., Grosz, A., Lineykin, S., Liverts, E., 2012. Modeling of small DC magnetic field response in trilayer magnetoelectric laminate composites. Adv. Condens. Matter Phys. 18, 383728.

ARTICLE IN PRESS

18   S. Rudykh, K. Bertoldi / J. Mech. Phys. Solids ∎ (∎∎∎∎) ∎∎∎–∎∎∎

Finally, defining $\xi = a_2/a_1$, Eq. (A.2) can be rewritten as

$$-(\mathcal{M}_{122}-(\mathcal{M}_{112}+\mathcal{M}_{121}-\mathcal{M}_{222})\xi-(\mathcal{M}_{122}+\mathcal{M}_{221}-\mathcal{M}_{111})\xi^2+\mathcal{M}_{121}\xi^3)^2+(\mathcal{A}_{2121}+\xi[2\mathcal{A}_{2122}-2\mathcal{A}_{1121}$$
$$+\xi(\mathcal{A}_{1111}-2\mathcal{A}_{1122}-2\mathcal{A}_{1221}+\mathcal{A}_{2222}+\xi(2\mathcal{A}_{1112}-2\mathcal{A}_{1222}+\mathcal{A}_{1212}\xi))])(\mathcal{H}_{22}+\xi(\mathcal{H}_{11}\xi-2\mathcal{H}_{12}))$$
$$= 0, \tag{A.3}$$

that can be reorganized in the form of a sextic polynomial as in Eq. (26) with the coefficients Γ_i is given by

$$\Gamma_0 = \mathcal{M}_{122}^2-\mathcal{A}_{2121}\mathcal{H}_{22},$$

$$\Gamma_1 = 2(\mathcal{A}_{2121}\mathcal{H}_{12}+(\mathcal{A}_{1121}-\mathcal{A}_{2122})\mathcal{H}_{22}-\mathcal{M}_{122}(\mathcal{M}_{112}+\mathcal{M}_{121}-\mathcal{M}_{222})),$$

$$\Gamma_2 = -\mathcal{A}_{2121}\mathcal{H}_{11}-4(\mathcal{A}_{1121}-\mathcal{A}_{2122})\mathcal{H}_{12}-(\mathcal{A}_{1111}-2\mathcal{A}_{1122}-2\mathcal{A}_{1221}+\mathcal{A}_{2222})\mathcal{H}_{22}$$
$$+2\mathcal{M}_{122}(\mathcal{M}_{111}-\mathcal{M}_{122}-\mathcal{M}_{221})+(\mathcal{M}_{112}+\mathcal{M}_{121}-\mathcal{M}_{222})^2,$$

$$\Gamma_3 = 2((\mathcal{A}_{1121}-\mathcal{A}_{2122})\mathcal{H}_{11}+(\mathcal{A}_{1111}-2\mathcal{A}_{1122}-2\mathcal{A}_{1221}+\mathcal{A}_{2222})\mathcal{H}_{12}$$
$$+(\mathcal{A}_{1222}-\mathcal{A}_{1112})\mathcal{H}_{22}+(\mathcal{M}_{121}\mathcal{M}_{122}-(\mathcal{M}_{111}-\mathcal{M}_{122}-\mathcal{M}_{221})(\mathcal{M}_{112}+\mathcal{M}_{121}-\mathcal{M}_{222}))),$$

$$\Gamma_4 = -(\mathcal{A}_{1111}-2\mathcal{A}_{1122}-2\mathcal{A}_{1221}+\mathcal{A}_{2222})\mathcal{H}_{11}+4(\mathcal{A}_{1112}-\mathcal{A}_{1222})\mathcal{H}_{12}$$
$$-\mathcal{A}_{1212}\mathcal{H}_{22}+(\mathcal{M}_{122}+\mathcal{M}_{221}-\mathcal{M}_{111})^2-2\mathcal{M}_{121}(\mathcal{M}_{112}+\mathcal{M}_{121}-\mathcal{M}_{222}),$$

$$\Gamma_5 = 2((\mathcal{A}_{1222}-\mathcal{A}_{1112})\mathcal{H}_{11}+\mathcal{A}_{1212}\mathcal{H}_{12}+\mathcal{M}_{121}(\mathcal{M}_{111}-\mathcal{M}_{122}-\mathcal{M}_{221})),$$

$$\Gamma_6 = \mathcal{M}_{121}^2-\mathcal{A}_{1212}\mathcal{H}_{11}. \tag{A.4}$$

References

Agoras, M., Lopez-Pamies, O., Ponte Castañeda, P., 2009. Onset of macroscopic instabilities in fiber-reinforced elastomers at finite strain. J. Mech. Phys. Solids 57, 1828–1850.

Bertoldi, K., Boyce, M.C., 2008. Wave propagation and instabilities in monolithic and periodically structured elastomeric materials undergoing large deformations. Phys. Rev. B 78, 184107.

Bertoldi, K., Gei, M., 2011. Instabilities in multilayered soft dielectrics. J. Mech. Phys. Solids 59, 18–42.

Biot, M.A., 1965. Mechanics of Incremental Deformations. John Wiley and Sons, New-York.

Brigadnov, I.A., Dorfmann, A., 2003. Mathematical modeling of magneto-sensitive elastomers. Int. J. Solids Struct. 40, 4659–4674.

Bruno, D., Greco, F., Lonetti, P., Blasi, P.N., Sgambitterra, G., 2010. An investigation on microscopic and macroscopic stability phenomena of composite solids with periodic microstructure. Int. J. Solids Struct. 47 (20), 2806–2824.

Bustamante, R., 2010. Transversely isotropic nonlinear magneto-active elastomers. Acta Mech. 210, 183–214.

Bustamante, R., Dorfmann, A., Ogden, R., 2006. Universal relations in isotropic nonlinear magnetoelasticity. Q. J. Mech. Appl. Math. 59, 435–450.

Chen, L., Gong, X.L., Li, W.H., 2007. Microstructures and viscoelastic properties of anisotropic magnetorheological elastomers. Smart Mater. Struct. 16, 2645–2650.

Chen, T., Nan, C.-W., Weng, G.J., 2003. Exact connections between effective magnetostriction and effective elastic moduli of fibrous composites and polycrystals. J. Appl. Phys. 94, 491–495.

Danas, K., Kankanala, S.V., Triantafyllidis, N., 2012. Experiments and modeling of iron-particle-filled magnetorheological elastomers. J. Mech. Phys. Solids 60, 120–138.

deBotton, G., 2005. Transversely isotropic sequentially laminated composites in finite elasticity. J. Mech. Phys. Solids 53, 1334–1361.

Deng, H., Gong, X., Wang, L., 2006. Development of an adaptive tuned vibration absorber with magnetorheological elastomer. Smart Mater. Struct. 15, N111–N116.

Destrade, M., Ogden, R.W., 2011. On magneto-acoustic waves in finitely deformed elastic solids. Math. Mech. Solids 16, 594–604.

Dorfmann, A., Ogden, R.W., 2004. Nonlinear magnetoelastic deformations. Q. J. Mech. Appl. Math. 57, 599–622.

Dorfmann, A., Ogden, R.W., 2005. Some problems in nonlinear magnetoelasticity. Z. Angew. Math. Phys. 56, 718–745.

Dorfmann, A., Ogden, R.W., 2010. Nonlinear electroelastostatics: incremental equations and stability. Int. J. Eng. Sci. 48, 1–14.

Farshad, M., Benine, A., 2004. Magnetoactive elastomer composites. Polym Test 23, 347–353.

Farshad, M., Le Roux, M., 2004. A new active noise abatement barrier system. Polym Test 23, 855–860.

Fleck, N., 1997. Compressive failure of fiber composites. Adv. Appl. Mech. 33, 43–117.

Galipeau, E., Ponte Castañeda, P., 2012. The effect of particle shape and distribution on the macroscopic behavior of magnetoelastic composites. Int. J. Solids Struct. 49, 1–17.

Galipeau, E., Rudykh, S., deBotton, G., Ponte Castañeda, P., Magnetorheological elastomers with periodic and random microstructures. Int. J. Solids Struct.(forthcoming).

Geymonat, G., Müller, S., Triantafyllidis, N., 1993. Homogenization of nonlinearly elastic materials, microscopic bifurcation and macroscopic loss of rank-one convexity. Arch. Ration. Mech. Anal. 122, 231–290.

Ginder, J.M., Clark, S.M., Schlotter, W.F., E., N.M., 2002. Magnetostrictive phenomena in magnetorheological elastomers. Int. J. Mod. Phys. B, 16, 2412–2418.

Ginder, J.M., Nichols, M.E., Elie, L.D., Clark, S.M., 2000. Controllable-stiffness components based on magnetorheological elastomers. Proc. SPIE 3985, 418.

Ginder, J.M., Schlotter, W.F., Nichols, M.E., 2001. Magnetorheological elastomers in tunable vibration absorbers. Proc. SPIE 4331, 103.

Gong, X.L., Zhang, X.Z., Zhang, P.Q., 2005. Fabrication and characterization of isotropic magnetorheological elastomers. Polym Test 24 (5), 669–676.

Guan, X., Donga, X., Ou, J., 2008. Magnetostrictive effect of magnetorheological elastomer. J. Magn. Magn. Mater. 320, 158–163.

Han, Y., Zhang, Z., Faidley, L., Hong, W., 2012. Microstructure-based modeling of magneto-rheological elastomers. In: Goulbourne, N., Ounaies, Z. (Eds.), Behavior and Mechanics of Multifunctional Materials and Composites, 2012, vol. 8342. . Proceedings of the SPIE, San Diego, CA, pp. 83421B.

Hill, R., 1957. On uniqueness and stability in the theory of finite elastic strain. J. Mech. Phys. Solids 5, 229–241.

Hill, R., Hutchinson, J.W., 1975. Bifurcation phenomena in the plane tension test. J. Mech. Phys. Solids 23, 239–264.

Hoang, N., Zhang, N., Du, H., 2011. An adaptive tunable vibration absorber using a new magnetorheological elastomer for vehicular powertrain transient vibration reduction. Smart Mater. Struct. 20, 015019.

Jolly, M.R., Carlson, J.D., Munoz, B.C., 1996. A model of the behaviour of magnetorheological materials. Smart Mater. Struct. 5, 607–614.

ARTICLE IN PRESS

S. Rudykh, K. Bertoldi / J. Mech. Phys. Solids ∎ (∎∎∎∎) ∎∎∎–∎∎∎   19

Kankanala, S.V., Triantafyllidis, N., 2008. Magnetoelastic buckling of a rectangular block in plane strain. J. Mech. Phys. Solids 56, 1147–1169.

Li, T., Keplinger, C., Baumgartner, R., Bauer, S., Yang, W., Suo, Z., 2013. Giant voltage-induced deformation in dielectric elastomers near the verge of snap-through instability. J. Mech. Phys. Solids 61, 611–628.

Lerner, A.A., Cunefare, K.A., 2008. Performance of MRE-based vibration absorbers. J. Intell. Mater. Syst. Struct. 19, 551–563.

Maugin, G.A., Eringen, A.C., 1972. Deformable magnetically saturated media, I. Field equations. J. Math. Phys. 13, 143–155.

Michel, J.C., Lopez-Pamies, O., Castañeda, P.P., Triantafyllidis, N., 2007. Microscopic and macroscopic instabilities in finitely strained porous elastomers. J. Mech. Phys. Solids 55, 900–938.

Nestorovic, M.D., Triantafyllidis, N., 2004. Onset of failure in finitely strained layered composites subjected to combined normal and shear loading. J. Mech. Phys. Solids 52, 941–974.

Otténio, M., Destrade, M., Ogden, R., 2008. Incremental magnetoelastic deformations, with application to surface instability. J. Elasticity 90, 19–42.

Ponte Castañeda, P., Galipeau, E., 2011. Homogenization-based constitutive models for magnetorheological elastomers at finite strain. J. Mech. Phys. Solids 59, 194–215.

Rudykh, S., Bhattacharya, K., deBotton, G., 2012. Snap-through actuation of thick-wall electroactive balloons. Int. J. Nonlinear Mech. 47, 206–209.

Rudykh, S., deBotton, G., 2011. Stability of anisotropic electroactive polymers with application to layered media. Z. Angew. Math. Phys. 62, 1131–1142.

Rudykh, S., deBotton, G., 2012. Instabilities of hyperelastic fiber composites: micromechanical versus numerical analyses. J. Elasticity 106, 123–147.

Thylander, S., Menzel, A., Ristinmaa, M., 2012. An electromechanically coupled micro-sphere framework: application to the finite element analysis of electrostrictive polymers. Smart Mater. Struct. 21 (9).

Tian, T.F., Li, W.H., Deng, Y.M., 2011. Sensing capabilities of graphite based MR elastomers. Smart Mater. Struct. 20, 025022.

Tiersten, H., 1964. Coupled magnetomechanical equations for magnetically saturated insulators. J. Math. Phys. 5 (9), 1298–1318.

Tiersten, H., 1965. Variational principle for saturated magnetoelastic insulators. J. Math. Phys. 6 (5), 779–787.

Triantafyllidis, N., Maker, B.N., 1985. On the comparison between microscopic and macroscopic instability mechanisms in a class of fiber-reinforced composites. J. Appl. Mech. Trans. ASME 52, 794–800.

Triantafyllidis, N., Nestorovic, M.D., Schraad, M.W., 2006. Failure surfaces for finitely strained two-phase periodic solids under general in-plane loading. J. Appl. Mech. Trans. ASME 73 (3), 505–515.

Truesdell, C., Toupin, R., 1960. The classical field theories. In: Handbuch der Physik, vol. III. Springer, Berlin.

Varga, Z., Filipcsei, G., Zrinyi, M., 2006. Magnetic field sensitive functional elastomers with tuneable elastic modulus. Polymer 47 (1), 227–233.

Wang, H., Cai, S., Carpi, F., Suo, Z., 2012. Computational model of hydrostatically coupled dielectric elastomer actuators. J. Appl. Mech. Trans. ASME 79 (3).

Zadov, B., Elmalem, A., Paperno, E., Gluzman, I., Nudelman, A., Levron, D., Grosz, A., Lineykin, S., Liverts, E., 2012. Modeling of small DC magnetic field response in trilayer magnetoelectric laminate composites. Adv. Condens. Matter Phys. 18, 383728.